### Title

A terminal metabolite of niacin promotes vascular inflammation and contributes to cardiovascular disease risk.




### Journal

Nature Medicine, 30(2)



### Authors

Ferrell, Marc

Wang, Zeneng

Anderson, James

et al.



### Publication Date

2024-02-01

### DOI

10.1038/s41591-023-02793-8

Peer reviewed

Published in final edited form as:

*Nat Med*. 2024 February ; 30(2): 424–434. doi:10.1038/s41591-023-02793-8.

# A terminal metabolite of niacin promotes vascular inflammation and contributes to cardiovascular disease risk

**Marc Ferrell**[1,2], **Zeneng Wang**[1], **James T. Anderson**[1], **Xinmin S. Li**[1], **Marco Witkowski**[1,14], **Joseph A. DiDonato**[1], **James R. Hilser**[3,4], **Jaana A. Hartiala**[3], **Arash Haghikia**[5,6,7,8,15], **Tomas Cajka**[9,10], **Oliver Fiehn**[9], **Naseer Sangwan**[1], **Ilja Demuth**[11,12], **Maximilian König**[11], **Elisabeth Steinhagen-Thiessen**[11], **Ulf Landmesser**[5,6,7,8,15], **W . H. Wilson Tang**[1,13], **Hooman Allayee**[3,4], **Stanley L. Hazen**[1,13,#]

[1]Department of Cardiovascular & Metabolic Sciences, Lerner Research Institute, Cleveland Clinic, Cleveland, OH

[2]Department of Nutrition, Systems Biology and Bioinformatics Program, Case Western Reserve University, Cleveland, OH

[3]Department of Population and Public Health Sciences, Keck School of Medicine, University of Southern California, Los Angeles, CA 90033, USA

[4]Department of Biochemistry & Molecular Medicine, Keck School of Medicine, University of Southern California, Los Angeles, CA 90033, USA

[5]Department of Cardiology, Angiology and Intensive Care, Deutsches Herzzentrum der Charité, Campus Benjamin Franklin, Berlin, Germany

[6]German Center for Cardiovascular Research (DZHK), Partner Site Berlin, Berlin, Germany

[7]Berlin Institute of Health (BIH), Berlin, Germany

[8]Friede Springer Cardiovascular Prevention Center at Charité, Berlin, Germany

[9]West Coast Metabolomics Center, University of California, Davis, Davis, California, USA

[#] Address for Correspondence: Stanley L. Hazen, MD, PhD, 9500 Euclid Avenue, NC-10, Lerner Research Institute, Cleveland Clinic, Cleveland, OH 44124, Fax: (216) 444-9404 / hazens@ccf.org.

Author Contributions

MF participated in the design, performance, and analysis of all studies presented, and drafted the manuscript with input from all authors. All authors participated in the preparation of the manuscript. ZW and XL performed mass spectrometry analysis. JA performed chemical synthesis. OF and TC performed untargeted metabolomics data acquisition. JRH, JAH, and HA performed and assisted in genomic analyses. JAD designed viral genomes. NS performed RNA sequencing analysis. AH, MW, ID, MK, EST, UL, and WHWT provided valuable insight on clinical studies. SLH conceived, supervised, and participated in the design of all studies presented.

Declaration of Interests

Drs Hazen and Wang report being named as co-inventors on pending and issued patents held by the Cleveland Clinic relating to cardiovascular diagnostics and therapeutics. Drs Hazen and Wang also report having received royalty payments for inventions or discoveries related to cardiovascular diagnostics or therapeutics from Cleveland Heart Lab, a fully owned subsidiary of Quest Diagnostics, and Procter & Gamble. Dr. Hazen is a paid consultant for Zehna Therapeutics and Proctor & Gamble, and has received research funds from Zehna Therapeutics, Proctor & Gamble, Pfizer, and Roche Diagnostics. Dr. Tang is a consultant for Sequana Medical A.V., Cardiol Therapeutics, Genomics plc, Zehna Therapeutics, and Renovacor, and has received honoraria from Springer Nature for authorship/editorship and American Board of Internal Medicine for exam writing committee. All other authors declare no competing interests.

Code Availability

Custom code is available at https://doi.org/10.5281/zenodo.8357441.

[10]Present address: Institute of Physiology of the Czech Academy of Sciences, Prague, Czech Republic

[11]Department of Endocrinology and Metabolism, Charité-Universitätsmedizin Berlin, Charitéplatz, Berlin, Germany

[12]Berlin Institute of Health Center for Regenerative Therapies, Berlin, Germany

[13]Department of Cardiovascular Medicine, Heart, Vascular and Thoracic Institute, Cleveland Clinic, Cleveland, OH

[14]Present address: Department of Cardiology, Angiology and Intensive Care, Deutsches Herzzentrum der Charité, Campus Benjamin Franklin, Berlin, Germany

[15]Charité – Universitätsmedizin Berlin, corporate member of Freie Universität Berlin and Humboldt-Universität zu Berlin, Charitéplatz 1, 10117 Berlin, Germany

## Abstract

Despite intensive preventive cardiovascular disease (CVD) efforts, substantial residual CVD risk remains even for individuals receiving all guideline-recommended interventions. Niacin is an essential micronutrient fortified in food staples, but its role in CVD is not well understood. Here, untargeted metabolomics analysis of fasting plasma from stable cardiac patients in a prospective Discovery Cohort (n=1,162 total, n=422 females) suggested niacin metabolism was associated with incident major adverse cardiovascular events (MACE). Plasma levels of the terminal metabolites of excess niacin, N1-methyl-2-pyridone-5-carboxamide (2PY) and N1-methyl-4-pyridone-3-carboxamide (4PY), were associated with increased 3-year MACE risk in two validation cohorts (US n=2,331 total, n=774 females; and European n=832 total, n=249 females) [adjusted hazard ratio(HR) (95% confidence interval), for 2PY: 1.64(1.10–2.42) and 2.02(1.29–3.18), respectively; for 4PY: 1.89(1.26–2.84) and 1.99(1.26–3.14), respectively]. Phenome-wide association analysis of a genetic variant, rs10496731, that was significantly associated with both 2PY and 4PY levels revealed an association of this variant with levels of soluble vascular adhesion molecule-1 (sVCAM-1). Further meta-analysis confirmed association of rs10496731 with sVCAM-1 (n=106,000 total, n=53,075 females, $P=3.6\times10^{-18}$). Moreover, sVCAM-1 levels were significantly correlated with both 2PY and 4PY in a Validation Cohort (n=974 total; n=333 females) (2PY, rho=0.13, $P=7.7\times10^{-5}$; 4PY, rho=0.18, $P=1.1\times10^{-8}$). Lastly, treatment with physiological levels of 4PY, but not its structural isomer 2PY, induced expression of VCAM-1 and leukocyte adherence to vascular endothelium in mice. Collectively, these results indicate that the terminal breakdown products of excess niacin, 2PY and 4PY, are both associated with residual CVD risk. They also suggest an inflammation-dependent mechanism underlying the clinical association of 4PY with MACE.

## Introduction

Cardiovascular disease (CVD) is a leading cause of morbidity and mortality worldwide [1], but only a portion of attributable risk is accounted for by established risk factors [2]. Despite significant advances in therapies, residual CVD risk remains high, suggesting additional yet unrecognized factors are involved in CVD. In randomized clinical trials of

PCSK9 (proprotein convertase subtilisin/kexin type 9) inhibitors, treatment groups achieved mean low-density lipoprotein (LDL) levels well below 50 mg/dL, but still had significant cardiovascular event rates [3,4]. In particular, subjects with elevated markers for inflammation have been noted to have increased residual CVD risks [5,6]. Here, we used an untargeted metabolomics approach to search for novel metabolites and pathways that might contribute to residual CVD risks. We used an untargeted mass spectrometry platform to screen for circulating small molecules whose levels predict incident CVD event risks independent of traditional risk factors. Herein we describe the discovery of clinical, genetic and mechanistic links between the terminal breakdown metabolites of excess niacin and incident risk for major adverse cardiac events (MACE).

Niacin, also known as vitamin B3 or nicotinic acid, is an essential micronutrient important for nicotinamide adenine dinucleotide (NAD) synthesis. While *de novo* synthesis and salvage pathways also contribute to the NAD pool, adults also require at least 15 mg per day to avoid niacin deficiency syndromes such as pellagra [7–9] (Figure 1a). In the mid-twentieth century during the Great Depression, heightened deaths from pellagra led to initially voluntary and then mandated niacin fortification of wheat flour and other cereals, and this mandate continues to the present (Code of Federal Regulations Section 21 § 136, 137, 139, Figure 1b). The niacin fortification mandate had its intended effect, a dramatic decline in pellagra deaths - so much so that monitoring of pellagra-induced mortality in the US was eventually stopped due to the rarity of the event [8] (Figure 1b). However, over the past half century, with consumption of increasing amounts of processed and “fast” foods (much of which include refined fortified flour and cereals), intake of dietary niacin has continued to increase to levels encroaching on excessive (i.e. the average niacin intake in the US is nearing the tolerable upper limit defined by the National Academy of Sciences [9], Figure 1b). In the most recent National Health and Nutrition Examination Surveys (NHANES) (2017-March 2020), respondents who completed both the diet and supplement surveys (n=1,703) reported more than adequate niacin intake (median(IQR), 37(27–50 mg)), and less than 4% reported <15 mg per day [10]. Therapeutic niacin (1,500–2,500 mg per day) was one of the first pharmacologic agents used for the treatment of dyslipidemia [11]; however, its efficacy for CVD risk reduction in the modern statin era has been questioned [12,13]. Recent clinical trials have shown that while niacin can reduce LDL cholesterol (and both raise high density lipoprotein cholesterol and lower triglycerides), in the setting of combined high potency statin therapy, niacin not only failed to diminish CVD risk [14,15], but in meta-analysis of the most recent trials, it even heightens overall mortality [16]. It has thus been recognized that niacin has a more complex effect on CVD events (the so-called “niacin-paradox”, wherein it lowers LDL cholesterol but not CVD event risks), presumably through mechanism(s) independent of cholesterol [13].

## Results

### Untargeted metabolomics as discovery platform for residual CVD risk.

In a prospective Discovery Cohort of stable participants undergoing elective diagnostic cardiac evaluation (n=1,162; Supplemental Table 2), untargeted metabolomics was performed to identify candidate metabolites associated with incident major adverse

cardiovascular events (MACE) independent of traditional CVD risk factors that might contribute to residual CVD risks. Of the metabolites associated with increased MACE risk, many are presumed lipids (including the phosphatidylethanolamines (PE) PE 38:4 and PE 36:2, Supplemental Table 3) or have known structures and have previously been associated with CVD risks (e.g. trimethyllysine [17], trimethylamine N-oxide [18], phenylacetylglutamine [19], and erythritol [20]). However, others could not be identified with database searches (i.e., "Unknowns"; Supplemental Table 4) and were only recognizable by their mass-to-charge ratio (*m/z*) and retention time. An analyte of unknown structure with high resolution *m/z* = 153.0656 Da, corresponding to an elemental composition of $C_7H_9O_2N_2$, was the top (ranking by adjusted hazard ratio) unknown metabolite associated with increased MACE risk (Supplemental Table 4). Individuals with higher circulating relative levels of this metabolite (we use the term "relative level" since untargeted metabolomics studies are only semi-quantitative) had increased incident MACE risk (4th vs other quartiles, Log-rank P<0.0001, Figure 2a). The increased risk of MACE associated with unknown analyte *m/z* = 153.0656 Da appeared to be independent of traditional CVD risk factors, since in Cox proportional hazards regression analyses, it remained significant (highest vs lowest quartile, hazard ratio (HR) (95% confidence interval (CI)): 2.77(1.59–4.86), P=0.0005; Figure 2b).

To gain further insights into the potential identity of unknown analyte *m/z* = 153.0656 Da and metabolic pathways it might be linked to, we further analyzed all of the untargeted metabolomics data using a network module-based pathway analysis approach designed for cross-sectional data (Methods, Extended Data Figure 1). This network module-based pathway approach identified several metabolic pathways with MACE-associated metabolites concentrated within a few enzymatic conversions of each other, indicating the overall pathways were associated with MACE. (Extended Data Figure 1, Supplemental Table 5). The "vitamin B3 [niacin/NAD] metabolism" module was associated with MACE and included two metabolites with predicted *m/z* values within measurement error of 153.0656 Da, the mass of the candidate unknown analyte most strongly associated with incident MACE (Extended Data Figure 2). Based upon this network module-based pathway analysis, we hypothesized that the candidate MACE-associated analyte with *m/z* = 153.0656 Da might not be a single molecule, but might instead be a mixture of two structural isomers that co-eluted (producing a blended mass spectrometry spectrum that was not recognized in existing databases) - specifically 2PY (N1-methyl-2-pyridone-5-carboxamide) and 4PY (N1-methyl-4-pyridone-3-carboxamide) (chemical structures shown in Figure 1a). Although previous reports indicate these two metabolites are produced from niacin/NAD [21] and their plasma levels are elevated when the niacin/NAD pool is in excess [21,22], little is known about these metabolites and their potential biological activities have rarely been studied. Chemical synthesis of authentic 2PY and 4PY standards (Methods, Supplemental Figures 1,2), and further chemical characterization studies (Methods, Extended Data Figures 3,4,5, Supplemental Figures 1,2, Supplemental Table 6), enabled unambiguous demonstration that the MACE-associated serum "analyte" with *m/z* = 153.0656 Da (elemental composition $C_7H_9O_2N_2$) was indeed a mixture of the co-eluting structural isomers 2PY and 4PY with identical elemental composition (Figure 2c–d, Extended Data Figures 4,5).

## Circulating levels of 2PY and 4PY, terminal metabolites of niacin metabolism, are linked to residual CVD risk.

Armed with a stable isotope dilution LC/MS/MS method to individually quantify 2PY and 4PY (i.e. baseline chromatographic separation, unique parent-daughter ion transitions, and synthetic heavy isotope (d3) labeled internal standards; Methods; Figure 2d; Extended Data Figure 4), we proceeded to test whether circulating levels of each structural isomer were associated with incident MACE risks in two distinct Validation Cohorts (US, n=2,331; and European, n=832, Supplemental Table 2). Kaplan-Meier analyses in each Validation Cohort showed subjects with higher circulating levels of either 2PY or 4PY had higher MACE risk ($4^{th}$ vs other quartiles, Log-rank P<0.05, Figure 3 a, b, c, d), and in Cox proportional hazards regression analyses, elevated 2PY or 4PY levels were associated with increased MACE risk in the highest vs lowest quartile after adjustment for established CVD risk factors. Similar results were observed in both the US Validation Cohort and the European Validation Cohort [adjusted hazard ratio(HR) (95% confidence interval (CI)), for 2PY: 1.64(1.10–2.42) and 2.02(1.29–3.18), respectively, and for 4PY: 1.89(1.26–2.84) and 1.99(1.26–3.14), respectively; Figure 3 e, f, g, h]. When renal function (eGFR) was added to the models, 4PY remained associated in both Validation Cohorts [adjusted HR(95% CI), 1.64(1.06–2.54) and 1.67(1.06–2.62) for the US and European Validation Cohorts, respectively], but 2PY was significantly associated only in the European Validation Cohort [adjusted HR(95% CI), 1.39(0.91–2.12) and 1.67(1.06–2.64) for the US and European Validation Cohorts, respectively].

Circulating levels of 2PY and 4PY were positively correlated with each other (Extended Data Figure 6a,b), as well as traditional CVD risk factors, including age, lipids, and renal function (Extended Data Figure 6c). 4PY was also positively correlated with CRP (Spearman rho=0.05, P=0.008). To further test for confounding with traditional risk factors, we performed sensitivity analysis across all samples in both Validation Cohorts. Both 2PY and 4PY remained associated with increased MACE risk in all sufficiently large subgroups examined with one exception. While elevated 4PY levels remain significantly associated with incident MACE risks both in subjects with relatively preserved renal function (eGFR $\geq$ 60 mL/min/1.73m$^2$, n=2,604) as well as those with impaired renal function (eGFR (< 60 mL/min/1.73m$^2$, n=552, interaction P = 0.2), the association observed with elevated 2PY levels and MACE risk was significantly attenuated by renal function (i.e., 2PY was only associated with MACE risk in those with impaired renal function, interaction P = $1.0\times10^{-11}$, Extended Data Figures 7a,b).

## Identification of ACMSD (aminocarboxymuconate semialdehyde decarboxylase) as a gene regulating 2PY and 4PY levels in humans and mice.

We next examined the genetic determinants of circulating 2PY and 4PY using a GWAS approach. In the US Validation Cohort, a GWAS analysis with over 9 million variants did not identify any variants that reached the genome-wide significance threshold that were associated with either 2PY or 4PY (Supplemental Figure 3). To increase statistical power, we carried out meta-analyses by combining our GWAS results in the US Validation Cohort with publicly available summary statistics for 2PY and 4PY levels from various multi-ancestry datasets (Supplemental Table 1). In total, 37,453 and 11,609 individuals

were included in the meta-analyses for 2PY and 4PY levels, respectively. The genomic control factors (λ) in both analyses were ≤1, indicating that the results of the meta-analyses were not confounded by underlying population stratification. As shown by the Miami plot in Figure 4a, levels of both 2PY ($P=1.6\times10^{-41}$) and 4PY ($P=7.2\times10^{-12}$) were associated with the same locus on chromosome 2. The lead variants for 2PY (rs10496731) and 4PY (rs6430553) both map within the gene encoding aminocarboxymuconate semialdehyde decarboxylase (*ACMSD*) and are in near perfect linkage disequilibrium (LD) with each other ($r^2=0.96$) (Figure 4b,c). Furthermore, the T and C alleles of rs10496731 and rs6430553 were consistently associated with increased levels of 2PY and 4PY, respectively, across all cohorts (Extended Data Table 1). Since association of both variants with 2PY and 4PY levels represent the same genetic signal, we focused our subsequent analyses on rs10496731. Based on the LC/MS/MS analyses in the US Validation cohort, each copy of the T allele of rs10496731 increased absolute levels of 2PY and 4PY levels by an average median of 0.225 μmol/L and 0.0335 μmol/L, respectively (Extended Data Table 2). Data from the Genotype-Tissue Expression (GTEx) project [23] further revealed that the T allele of rs10496731 was associated with reduced ACMSD activity by altering abundance of functional splice variants (Figure 4d, Methods).

To directly test the hypothesis that ACMSD regulates 2PY and 4PY levels, we knocked down *Acmsd* expression *in vivo* by injecting mice with a liver-tropic AAV expressing either an shRNA targeting *Acmsd* or a scrambled control shRNA. Four weeks after injection, *Acmsd* mRNA and protein levels in livers of mice receiving the *Acmsd* shRNA AAV were significantly reduced by 41% and 37%, respectively, compared to mice receiving the AAV expressing scrambled shRNA (Figure 4e,f and Supplemental Figure 4). Serum levels of 2PY and 4PY were also both increased by 3.6-fold and 49%, respectively, in mice injected with *Acmsd* shRNA AAV (Figure 4g). Taken together, these data functionally validate *ACMSD* as playing a role in the metabolism of 2PY and 4PY in both mice and humans.

## Genetic, clinical, and functional association of 4PY with VCAM-1 levels.

We next used a PheWAS approach to identify a putative biological mechanism for association of 2PY and 4PY levels with increased risk of MACE. We focused our search on metabolomic and proteomic markers that were also associated with rs10496731 since such traits would be biologically closest to our metabolomics-level data. Several proteins and metabolites were associated with rs10496731 in the PheWAS analyses, which we prioritized as described in Supplemental Table 7. Based on these analyses and prioritization strategy, we focused on VCAM-1 since rs10496731 reproducibly yielded directionally consistent association with sVCAM-1 levels in multiple GWAS datasets [24,25] (Supplemental Table 7). VCAM-1 is a known participant in vascular inflammation and atherogenesis [26,27], further strengthening the prioritization of this candidate for functional follow up studies. To further confirm association of rs10496731 with sVCAM-1 levels, we measured serum sVCAM-1 in a subset of 974 sequential samples from the US Validation Cohort. Among these subjects, sVCAM-1 levels were associated with increased MACE risk [adjusted hazard ratio, HR(95% confidence interval), 2.38(1.14–4.95), P=0.02, Supplemental Figure 5a–b] and with rs10496731 (P=0.02, Extended Data Table 2). Furthermore, sVCAM-1 levels were

also correlated with circulating levels of both 2PY (Spearman rho=0.13, $P=7.7\times10^{-5}$) and 4PY (Spearman rho=0.18, $P=1.1\times10^{-8}$) (Figure 5a,b).

We next performed a meta-analysis with rs10496731 and sVCAM-1 levels by combining our association results in the US Validation Cohort, with those we carried out with proteomics data in the UK Biobank [28] and publicly available summary statistics from various other cohorts (combined n=106,000) (Extended Data Table 1, Supplemental Table 1). These analyses further confirmed significant association of rs10496731 with circulating sVCAM-1 levels ($P=3.6\times10^{-18}$, Extended Data Table 1) and suggested that 2PY and/or 4PY could be associated with risk of MACE through this known vascular inflammation CVD biomarker.

We also evaluated whether genetically increased 2PY and 4PY levels were causally associated with CVD outcomes using MR analyses. For this purpose, the effect sizes of the T allele of rs10496731 on 2PY and 4PY levels obtained from our meta-analysis were used for the exposure and the effect estimates derived from our analysis of rs10496731 with risk of incident MACE in the UK Biobank, as well as those obtained from publicly available summary statistics for CAD [29], MI [30], and stroke [31], were used for the outcomes. However, MR analysis did not provide evidence for a causal association between genetically increased 2PY and 4PY levels and risk of MACE, CAD, MI, or stroke (Supplemental Table 8).

**4PY, but not 2PY, is biologically active and provokes vascular inflammation and leukocyte adhesion.—**Direct functional testing is the strongest data to support a link between 2PY/4PY and VCAM-1. Thus, we next carried out a series of *in vitro* and *in vivo* functional experiments to explore whether 2PY or 4PY, at physiological levels, would elicit expression of VCAM-1 on endothelial cells. Human vascular endothelial cells were incubated with either 2PY, 4PY, vehicle control, or LPS as a positive control. Notably, a physiological level of 4PY, but not 2PY, provoked mRNA and protein expression of VCAM-1 on human endothelial cells (Figure 5c,d). In a second independent experiment, we also performed transcriptomics analysis to identify other pathways potentially affected by 2PY or 4PY in endothelial cells. In addition to replicating the effect of 4PY on upregulating *VCAM1* mRNA levels, expression of individual genes, such as *BEST1* and *RNY1*, were specifically altered by incubation with 4PY (Extended Data Figure 8a,b,c). Bioinformatics analyses with differentially expressed genes also revealed enrichment of various pathways related to transcriptional regulation and *WNT* signaling, including upregulation of genes involved in the cellular response to tumor necrosis factor, such as *AKT1, MAPK3,* and *VCAM1* (Extended Data Figure 8d,e).

Finally, we used an *in vivo* approach to test whether 2PY or 4PY have acute effects on arterial VCAM-1 expression and function. Pharmacokinetic studies indicated intraperitoneally administered 2PY and 4PY have half-lives of approximately 1 hour (Supplemental Figure 6). Thus, mice were injected with 2PY, 4PY, or vehicle control after zero, two, and four hours to ensure circulating levels remained elevated long enough for VCAM-1 protein to be potentially expressed in response (Supplemental Figure 6). Six hours after the first injection, endothelial VCAM-1 expression on aortic endothelial cells was elevated by 4PY, but not 2PY (Figure 5e,f), consistent with our findings *in vitro*. In further functional studies, we tested whether 4PY treatment (but not 2PY) would enhance

leukocyte adherence to the vessel wall *in vivo* (a prototypic *in vivo* function of VCAM-1). Following similar exposure to 4PY, 2PY or vehicle, intravital microscopy analysis showed that physiological levels of 4PY, but not 2PY or vehicle, increased the numbers of adherent leukocytes in auricular venules (Figure 5g,h).

## Discussion

Despite advances in preventive cardiovascular efforts, substantial residual CVD risk remains. Efforts to identify potential pathways linked to residual CVD risks remain a top priority. In the present studies, through use of untargeted metabolomics as a discovery platform, and subsequent structural elucidation studies coupled with multiple validation, genetic and vascular functional studies, we show that two terminal metabolites of niacin and NAD metabolism are both clinically associated with CVD independent of traditional risk factors, and both metabolites are also genetically linked to vascular inflammation (Scheme illustrating pathway/findings is shown in Figure 6). Niacin, which is fortified in food staples, contributes to NAD synthesis, and has been shown to provoke increased circulating 2PY and 4PY when present in excess, such as when provided as an over-the-counter supplement, or as pharmacological agent for cholesterol lowering [7,21,22] (Figure 6). NAD is also synthesized *de novo* via a pathway regulated by the enzyme ACMSD. Our GWAS and other functional studies reveal a variant within this gene that is significantly associated with both circulating 2PY and 4PY levels, as well as sVCAM-1 levels. Notably, direct provision of 4PY, but not the structural isomer 2PY, to vascular endothelial cells and to mice directly fostered enhanced endothelial cell activation and expression (both RNA and protein) of VCAM-1. The present studies thus suggest that the terminal metabolites of excess niacin, especially 4PY, are associated with incident MACE risks, and may be linked to the pathogenesis of residual CVD risk via inflammatory pathways including direct enhancement in VCAM-1 expression.

Although its role in CVD is incompletely understood, niacin remains a commonly used over-the-counter supplement [32]. Moreover, its use as supplement has increased over the years and it remains incorporated into the base of the food pyramid of countries like the US where flour, cereal and rice fortification mandates exist [33]. While no longer part of mainstream guideline recommendations [34–36], niacin was among the first lipid-lowering drugs. The Coronary Drug Project (conducted 1966 to 1975) was a randomized clinical intervention study that first demonstrated its efficacy in reducing total cholesterol along with modest reduction in CVD events among higher risk subjects [11]. However, more recent placebo controlled randomized trials of niacin conducted in the presence of first-line statin therapy (HPS2-THRIVE and AIM-HIGH) failed to demonstrate efficacy despite further decreases in LDL cholesterol (and increases in HDL cholesterol) in the niacin treatment groups [14,15]. Moreover, upon meta-analysis of these more recent trials, niacin was observed to increase total mortality [16]. In addition, in the AIM-HIGH trial, the rate of ischemic stroke was higher in the niacin group (HR (95% CI): 1.78 (1.00 – 3.17), P=0.05) [15,37]. Whether elevated niacin metabolites including 2PY and/or 4PY and associated vascular inflammation contribute to the observed excess mortality or other adverse events in these studies remains to be determined.

Niacin is ubiquitous in Western diets, with dietary reference intakes that vary with age and sex (RDAs 14 – 18 mg) [9]. The US and over 50 other nations mandate niacin fortification in staple foods to prevent pellagra despite the wide availability of foods naturally rich in niacin (i.e. 6 oz of tuna or 4 oz of peanuts contain 100% of the dietary reference intake for niacin [38]). In addition to food, 36% of US residents reported taking dietary supplements containing niacin on NHANES surveys from 1999 to 2010 [32]. The USDA estimates that total niacin consumption averaged 35 mg per day in 2010 [39] and NHANES surveys from 2017 to March 2020 averaged 48 mg per day [10] – more than triple the RDA [9]. In addition to niacin, it is noteworthy that 2PY and 4PY are also raised by the NAD-raising molecules nicotinamide riboside and nicotinamide mononucleotide [40–42], both of which are commonly sold supplements with claimed anti-aging benefits, although clinical trials remain mostly incomplete [43–47]. The present studies suggest niacin pool supplementation may optimally require a more nuanced titrated approach to achieve intended health benefits (e.g. monitoring for repletion of NAD pool members while not fostering excess 4PY generation).

As illustrated in Figure 6, NAD – an important cofactor in hundreds of enzymatic reactions – is synthesized from niacin or tryptophan, and its catabolism produces 2PY and 4PY. The intracellular niacin/NAD pool is tightly regulated, with several mechanisms of synthesis and degradation. New NAD is synthesized from dietary niacin and tryptophan, although niacin is the major contributor in humans [7]. Several enzymes cleave NAD, releasing nicotinamide, which can be rapidly recycled to resynthesize NAD. However, in a state of excess NAD/niacin pool, nicotinamide is increasingly catabolized to form the terminal metabolites 2PY and 4PY, which are then excreted renally [48,49] (Figure 6). In humans, a small fraction of dietary tryptophan is converted to NAD [50]. Furthermore our, genomic analyses revealed an association between 2PY and 4PY levels and a functional genetic splice variant of *ACMSD*, an enzyme regulating tryptophan-NAD conversion [51,52], which was validated with our *in vivo Acmsd* knockdown experiments. Taken together, these data suggest that genetically reduced functional *ACMSD* capacity in humans or mice shunts the intermediate tryptophan metabolite aminocarboxymuconate semialdehyde towards production of quinolate, nicotinamide metabolites, and, ultimately, 2PY and 4PY. Consistent with this model, the T allele of rs10496731 was also significantly associated with increased levels of both quinolinate and 1-methylnicotinamide [53]. While MR analyses did not provide evidence for genetically elevated 2PY or 4PY levels being causally associated with CVD events, we note these negative findings may have been due to the rs10496731 variant being a weak genetic instrument [54]. For example, the modest effect of the T allele of rs10496731 on 2PY and 4PY levels would not shift an individual from one quartile to the next. Thus, our MR analysis had less than 5% power to detect association with risk of CAD as a representative outcome.

Vascular inflammation is a critical component of CVD. The landmark CANTOS trial established a causal link between inhibition of inflammation via the interleukin 1 pathway and decreased CVD event risk [55]. Intimal plaque consists largely of macrophages recruited to the vessel wall by luminal proteins displayed by the vascular endothelium [56,57]. One such luminal protein, VCAM-1, is induced by interleukin 1β [58], and in preclinical models, genetic knockdown of VCAM-1 protected animals from atherosclerosis [26,27]. A portion of endothelial VCAM-1 is released as sVCAM-1, which is measurable in blood, and

circulating sVCAM-1 levels are associated with increased incident CVD risk [59,60]. In this regard, sVCAM-1 was also associated with MACE in the US Validation Cohort and our genetic analyses demonstrated the genome-wide significant variant for circulating 2PY and 4PY levels, rs10496731, was also highly associated with sVCAM-1 levels. These latter observations were validated through our functional *in vitro* and *in vivo* experiments, which demonstrated that 4PY, but not 2PY, directly fostered VCAM-1 mRNA and protein expression, and promoted the prototypic VCAM-1 function, leukocyte adhesion to vascular endothelium [26,27].

We note several limitations of our study. Measurement of 2PY and 4PY in the Validation Cohorts was only performed once, with samples drawn following an overnight fast at the time of enrollment. Whether serial measures would provide enhanced prognostic value for incident CVD risks remains unknown. In addition, our cohorts were recruited at quaternary referral centers and show a high prevalence of CVD and cardiometabolic disease risk factors. Further, while the meta-analysis of community-based genomic studies performed show a link between 4PY and VCAM-1 expression in multiple ethnic groups, the clinical studies linking 4PY to CVD events presented are based on high-risk European ancestry populations in the US and Europe Cohorts studied. The translatability of our findings to both community-based cohorts with lower overall CVD and metabolic disease risk, and alternative ethnicities, requires further study. We also recognize that clinical observational studies by design only show association, and not causation; thus, there always exists the possibility of unmodelled confounding that may have impacted our results through factors that are not included in our models (for example, we have no information on dietary niacin intake). However, to address this issue we also performed additional genetic, *in vitro* and animal model mechanistic studies with 2PY and 4PY. These revealed a link with vascular inflammation, and a direct effect of 4PY *in vivo* was shown. Both cellular and *in vivo* studies indicate that 4PY can serve as a driver of vascular inflammation and vascular phenotypes relevant to CVD initiation and pathogenesis. Long-term studies will be needed to test the effect of chronic 4PY elevation on phenotypes such as atherosclerosis. Collectively, the present studies provide evidence suggesting the clinical associations observed for 4PY and MACE risks may arise from an underlying causal connection between this terminal niacin metabolite and CVD relevant phenotypes. In contrast to 4PY, the association between 2PY and MACE appears confounded by renal function and is likely due to its high correlation with 4PY (2PY is co-produced with its structural isomer 4PY by the same enzyme in the presence of niacin pool excess).

In summary, the present studies, combined with recent randomized clinical trials with niacin in the modern era of high potency statins [14,15], suggest a possible explanation for the “niacin paradox” - the observation that the LDL lowering induced by niacin fails to achieve the expected reduction in CVD risks. The present studies also raise the question of whether a continued mandate of flour and cereal fortification with niacin is warranted. While such a mandate no doubt saved lives when first implemented >80 years ago, its long-term safety, particularly in more vulnerable populations, merits discussion (e.g. should easing of the mandate to allow “organic” or “non-fortified” flour and cereal options be available - particularly given the highest quartile of 4PY levels is associated with an approximately 2-fold increased incident MACE risk compared to those harboring lowest

quartile levels). The present studies suggest further investigation of the links between niacin/NAD supplementation, 4PY and atherosclerotic cardiovascular disease are needed.

## Methods

### Ethics Approvals

All human subjects gave written informed consent, and all human studies performed abided by the Declaration of Helsinki. The Institutional Review Board of the Cleveland Clinic, or the ethics committee of Charité-Universitätsmedizin Berlin, approved all study protocols (GeneBank IRB 4265, European Validation Cohort EA1/135/16).

### Clinical Cohorts

An initial Discovery Cohort (n=1,162; for untargeted metabolomics analyses) and a subsequent non-overlapping Validation Cohort (US Validation Cohort, n=2,331; for quantitative stable isotope dilution high performance liquid chromatography with online tandem mass spectrometry [LC/MS/MS] analyses of 2PY and 4PY) used archival fasting samples from GeneBank at the Cleveland Clinic, an observational cohort study with adjudicated longitudinal outcome data (GeneBank: NCT00590200 https://clinicaltrials.gov/ct2/show/NCT00590200) [17–20,61,62]. GeneBank has a large geographic catchment (significant out of state enrollment, with 48 of 50 US states represented amongst enrolling subjects) from a quaternary referral center and is comprised of sequential consenting stable subjects undergoing elective diagnostic cardiac evaluations. Exclusion criteria for GeneBank included myocardial infarction within the preceding four weeks of enrollment, or elevated troponin I (>0.03 mg/dL; Abbott Architect) at enrollment. MACE was defined as death from any cause, nonfatal myocardial infarction, or nonfatal stroke following enrollment [17–20,61,62]. For the present studies, in the US Validation Cohort, subjects with evidence of (prescriptive) niacin use at time of enrollment or within the preceding 30 days were excluded. In a sequential subset of the US Validation Cohort (n=974 sequential subjects), sVCAM-1 was measured by enzyme-linked immunosorbent assay (ELISA) (Invitrogen, Waltham, MA, Cat. # KHT0601). In the Discovery Cohort, alcohol use data was missing for 22 subjects (1.9%), and high sensitivity C-reactive protein (CRP) levels and current smoking status were missing for two subjects (<1%). In the US Validation Cohort, lipid profiles were missing for 10 subjects (<1%), current smoking status was missing for 9 subjects (<1%), and high sensitivity CRP levels were missing for 329 subjects (14%).

A second Validation Cohort (European Validation Cohort, n=832) was used for quantitative stable isotope dilution LC/MS/MS analyses of 2PY and 4PY on archival fasting samples from sequential stable patients undergoing elective diagnostic coronary angiography with adjudicated longitudinal outcome data as part of the observational LipidCardio study (German Clinical Trial Register (drks.de). Identifier: DRKS00020915). LipidCardio subjects have broad geographic catchment with residences throughout Europe, and all enrollment (2016–2018) occurring from the quaternary referral center Charité University Hospital, Campus Benjamin Franklin [63]. In the European Validation Cohort, high sensitivity CRP levels were missing for one subject (<1%), education level was missing for 398 subjects

(~48%), and lipid profiles were incomplete (did not include triglycerides) in 252 subjects (~30%).

Estimated glomerular filtration rate (eGFR) in both US and European Validation Cohorts was calculated as previously described [64] with analyses examined above versus below the cut point for chronic kidney disease stage IIIa (<60 mL/min/1.73m$^2$). Further details of untargeted metabolomics and stable isotope dilution LC/MS/MS analyses are provided in Materials. All sample sizes (n) presented represent measurements of distinct tissue samples from distinct individuals.

This manuscript was prepared in compliance with the Strengthening the Reporting of Observational studies in Epidemiology (STROBE)-Statement [65].

## Untargeted LC/MS/MS Metabolomics

Untargeted analysis of plasma samples was conducted at the West Coast Metabolomics Center (Davis, CA) using a previously described assay [17,19]. Polar metabolites were extracted from a plasma sample (30 μL) following protein precipitation using an acetonitrile/isopropanol/water (3:3:2, v/v/v) mixture (1 mL). Aliquots (300 μL) were evaporated, resuspended using an acetonitrile/water (4:1, v/v) mixture (60 μL) containing a series of deuterated internal standards, vortexed, centrifuged, and 50 μL supernatant was transferred to a glass vial with a microinsert. Hydrophilic interaction chromatography (HILIC) analysis was performed on a system including an Agilent 1290 Infinity LC system (Agilent Technologies) with a pump (G4220A), a column oven (G1316C), an autosampler (G4226A), and a TripleTOF 5600+ (SCIEX). Extracts were separated (Extended Data Figure 4) on an Acquity UPLC BEH Amide column (150 × 2.1 mm; 1.7 μm, Waters) coupled to a Waters Acquity UPLC BEH Amide VanGuard precolumn (5 × 2.1 mm; 1.7 μm). The column was maintained at 45°C at a flow rate of 0.4 mL/min. The mobile phases consisted of (A) water with ammonium formate (10 mM) and formic acid (0.125%) and (B) 95:5 (v/v) acetonitrile/water with ammonium formate (10 mM) and formic acid (0.125%). The separation was conducted using the following gradient: 0 min 100% B; 0–2 min 100% B; 2–7.7 min 70% B; 7.7–9.5 min 40% B; 9.5–10.25 min 30% B; 10.25–12.75 min 100% B; 12.75–17.75 min 100% B. A sample volume of 1 μL was used for the injection. Sample temperature was maintained at 4°C. The QTOF-MS instrument was operated with electrospray ionization in positive ion mode with the following parameters: curtain gas, 35 psi; ion source gas 1, 50 psi; ion source gas 2, 50 psi; temperature, 300°C; ion spray voltage floating, 4.5 kV; declustering potential, 100 V; acquisition speed, 2 spectra/s. For data processing, MZmine 2 [66] and MultiQuant software programs were used.

## Pathway Analysis of Untargeted Metabolomics Measurements

The mummichog algorithm was used for network module-based pathway analysis as implemented in the Metaboanalyst v4.0 (www.metaboanalyst.ca) Peaks to Pathways function [67,68]. This algorithm uses a network inference approach to map metabolites with undetermined structures to pathways. The Human MetaFishNet (MFN) genome-scale metabolic model, as released with Metaboanalyst v4.0, was used as the reference [68]. Human MFN was derived from Kyoto Encyclopedia of Genes and Genomes (KEGG) release 81.0,

Small Molecule Pathway Database (SMPDB) v2.0, Human Metabolome Database (HMDB) v4.0, Chemical Entities of Biological Interest (ChEBI) release 131, and Biocyc release 17.0 [67]. The mummichog method is described briefly below and has been extensively described previously [67].

Previously, Human MFN was constructed as a network (also known as a graph) by defining all human metabolites listed in KEGG, SMPDB, HMDB, ChEBI, and Biocyc as points (nodes) and all chemical reactions (enzymatic or otherwise) as connections (edges) between metabolites. Thus, any two molecules (nodes) participating in the same enzymatic reaction are connected with a line (edge).

All metabolites detected during metabolomics are compared between cases and controls using t statistics. Unadjusted P values determined using student's t tests compared between cases and controls are used to label each metabolite significant or not significant. High-resolution *m/z* measures are searched against the Human MFN database, resulting in zero, one, or multiple matches for each detected metabolite.

Mummichog extracts the network modules from Human MFN that maximize Newman-Girvan modularity among detected molecules. Due to the natural structure of metabolic conversions, extracted modules correspond to metabolic pathways. Mummichog's activity score for each pathway (module) is the product of Newman-Girvan modularity $Q$ and the fraction of metabolites (nodes) labeled as significant. The null distribution of a pathway's activity score is modelled with a gamma distribution constructed via maximum likelihood optimization using resampled subsets of all detected molecules (resampled until goodness-of-fit thresholds are met). The P value for pathway association is then calculated from the cumulative distribution function of the null distribution.

To prioritize unidentified metabolites for structural elucidation, this network module-based pathway analysis was used to identify metabolic pathways associated with MACE (Supplemental Table 5). This technique is based on the assumption that correct structural assignments for disease-associated metabolites (nodes) are likely to be concentrated in a subset of pathways (modules) associated with disease, thus structural assignments within MACE-associated pathways (modules) are likely to be correct [67]. For structural studies, we prioritized unidentified metabolites (nodes) associated with MACE whose related metabolic pathways were also associated with MACE and used traditional chemistry methods to confirm the putative structures suggested during pathway analysis. Eight such metabolite-pathway pairs could be identified, including several previously described metabolite-CVD associations (Extended Data Figure 1, Supplemental Table 5). Beta-alanine metabolism (driven by spermidine), lysine metabolism (driven by trimethyllysine), and branched-chain amino acid metabolism (driven by 3-aminoisobutanoate) have previously been associated with CVD [17,69–71] and were also associated in our network module-based pathway analysis. The only metabolite-pathway pair that included an unidentified metabolite was niacin (vitamin B3) metabolism (Extended Data Figure 2), driven by an unidentified plasma metabolite (observed *m/z* = 153.0656 Da, Supplemental Table 4). This unidentified plasma metabolite with *m/z* = 153.0656 Da was the top MACE-associated unknown (by hazard ratio, Supplemental Table 4) and was putatively assigned to both 2PY and 4PY (predicted

*m/z* = 153.0664 Da, Figure 2, Extended Data Figure 2, Supplemental Table 5). This plasma metabolite was prioritized for structural studies.

## Structural Elucidation of a Mass Spectral Feature Associated with MACE Risk (m/z = 153.0656)

The plasma metabolite (*m/z* = 153.0656 Da) appeared to be a mixture of 2PY and 4PY. The metabolite's collision-induced dissociation (CID) spectrum included daughter fragments characteristic of synthetic 2PY and 4PY (Extended Data Figure 3a).

Before making efforts to separate the plasma metabolite (*m/z* = 153.0656 Da) into multiple fractions, a "gut check" was performed to test whether the plasma metabolite (*m/z* = 153.0656 Da) CID could be reproduced from a mixture of synthetic 2PY and 4PY. Analysis of mixtures of authentic standard material showed the ratio of characteristic CID fragments could be used to calibrate the molar ratio of 2PY to 4PY in solution (Extended Data Figure 3b–c). The 2PY:4PY ratio was estimated in three human serum samples, and the estimated molar ratio was prepared in deionized water with authentic standards. The CID spectrum generated from the mixture of 2PY and 4PY was similar to the CID generated from the unknown metabolite (*m/z* = 153.0656 Da) in plasma (Extended Data Figure 3d). We next used chromatography to test whether the unknown metabolite with *m/z* = 153.0656 Da could be separated into multiple fractions.

2PY and 4PY are structural isomers, and they have the same predicted mass to charge ratio (*m/z*) and were not resolved with the amide column used for untargeted metabolomics (Extended Data Figure 4). A new chromatography method was developed to resolve 2PY and 4PY with a silica hydrophilic interaction liquid chromatography (HILIC) column, and this method demonstrated two baseline separated chromatographic peaks when monitoring a shared parent-to-daughter ion transition (*m/z* 153 → 108 Da, Extended Data Figure 4). These two peaks were identified as 2PY and 4PY based on multiple reaction monitoring (MRM) parent-to-daughter ion transitions with selectivity for 2PY and 4PY (Extended Data Figure 4, *m/z* 153 → 110 Da and 153 → 136 Da, respectively). These parent-to-daughter ion transitions were detectable in plasma and coeluted with synthetic 2PY and 4PY, as well as stable-isotope labeled d3–2PY (N1-methyl-(d3)-2-pyridone-5-carboxamide) and d3–4PY (N1-methyl-(d3)-4-pyridone-3-carboxamide) (Extended Data Figure 4, *m/z* 156 → 113 Da and 156 → 139 Da, respectively). Additional parent-to-daughter ion transitions characteristic of both 2PY and 4PY were detectable in plasma and co-eluted with their corresponding synthetic 2PY and 4PY isotopologues (Extended Data Figure 4). Finally, high resolution CID spectra were acquired for each peak separately, and the spectra produced by serum analytes were identical to those produced by synthetic 2PY and 4PY (Extended Data Figure 5, Supplemental Table 6). Our new HPLC method, described in greater detail below, was employed for stable isotope dilution LC/MS/MS quantitation of 2PY and 4PY in the Validation Cohort.

## Chemical Synthesis

Common and International Union of Pure and Applied Chemistry (IUPAC) names are given below. All solvents and reagents were purchased from commercial sources and used without

additional purification. Commercial sourcing of reagents: 4-chloronicotinic acid (Ambeed, Cat# A229266), 6-oxo-1,6-dihydropyridine-3-carboxylic acid (Ambeed, cat# A297691), dimethyl sulfate (Thermo Scientific, Cat# 430831000), N-methylmorpholine (Thermo Scientific, Cat# 127151000), dimethylformamide (Thermo Scientific, Cat# 326870025), isobutyl chloroformate (Acros Organics, Cat# 176181000), aqueous ammonium hydroxide (Avantor J.T. Baker, Fisher Scientific Cat# 02–002-290), methanol (Fisher Scientific, Cat# A454–4), dichloromethane (Fisher Scientific, Cat# D37–4), triethylamine (Sigma-Aldrich, Cat# T0886), thionyl chloride (Thermo Scientific, Cat# 041868.36). The temperature given for each experiment refers to the media used to warm (silicone oil) or cool (ice bath) the reaction vessel unless otherwise noted. 1H-nuclear magnetic resonance (1H-NMR) spectra were recorded using a Bruker Ascend spectrometer operating at 400 MHz. 1H-NMR data are reported as follows: chemical shift (δ in parts per million), multiplicity, coupling constant(s) (hertz), and number of protons. Multiplicities are represented as: s, singlet; br s, broad singlet; d, doublet; t, triplet; q, quartet; dd, doublet of doublets; ddd, doublet of doublets of doublets; dt, doublet of triplets; td, triplet of doublets; dq, doublet of quartets; and m, multiplet. Low-resolution mass measurements (*m/z*) were carried out using a Finnigan LTQ mass spectrometer using direct injection. High-resolution mass measurements (*m/z*) were carried out either by direct injection using a Thermo QExactive mass spectrometer or a tandem LC/MS system using an Agilent1290 Infinity II (LC)--Agilent 6230 TOF mass spectrometer. All isolated compounds were dried under vacuum until a constant weight was achieved.

### N1-methyl-4-pyridone-3-carboxamide (4PY, IUPAC 1-Methyl-4-oxo-1,4-dihydropyridine-3-carboxamide)

**4-hydroxynicotinic acid:** A mixture of 4-chloronicotinic acid (32.70 g, 207.6 mmol) in water (280 mL) was stirred at 105 °C (oil bath temperature) for 2.5 h whereupon the reaction mixture became homogeneous. Mass spec showed a clean complete reaction and desired product [M+H]+ = 140 Da. Reaction mixture cooled to room temperature and then stirred in an ice bath whereupon an off-white precipitate formed. 6 M aqueous sodium hydroxide (34.5 mL, 207 mmol) was slowly added over a period of 10 min to neutralize the hydrochloric acid formed. Additional off-white precipitate also formed upon neutralization. Mixture sat in an ice bath for 15 min. The off-white solid was suction filtered through grade 1 filter paper, rinsed with cold water (75 mL), and then dried under high vacuum overnight to give 4-hydroxynicotinic acid, 25.19 g, 87% yield. Material used as is despite 1H-NMR showing 2-sets of additional minor peaks.

1H-NMR major component (400 MHz, DMSO-d6): δ 12.89 (br s, 1H), 8.61 (s, 1H), 8.08 (d, J = 7.1 Hz, 1H), 6.73 (d, J = 7.1 Hz, 1H)

1H-NMR minor components (assumed to be 2 components at ~5 mol% each) (400 MHz, DMSO-d6): δ 15.92 (br s), 9.25 (s), 9.00 (d, J = 4.8 Hz), 8.83 (s), 8.31 (d, J = 7.1 Hz), 7.84 (d, J = 4.8 Hz), 6.86 (d, J = 7.1 Hz), −3.99 (br s)

**1-methyl-4-oxo-1,4-dihydropyridine-3-carboxylic acid:** Dimethyl sulfate (120 mL, 1268 mmol) was added to 4-hydroxynicotinic acid (48.41 g, 348.0 mmol) and the resulting

heterogeneous mixture stirred and heated to 100°C (oil bath temperature). The solid mixture started to thin after 30 min. The mixture stirred at 100 °C for 2.5 h whereupon a brown homogeneous solution had formed. Reaction mixture cooled to room temperature and then 6 M aqueous sodium hydroxide (~300 mL) was slowly added over a period of 20 min until pH ~12 was achieved. A precipitate was observed after ~60 mL of the 6 M sodium hydroxide solution was added but dissolved upon further addition of 6 M sodium hydroxide. Resulting solution stirred and heated to ~65 °C (internal temperature) for 10 min and then cooled to room temperature. Reaction mixture was partially concentrated using rotary evaporation to remove methanol (~90 mL) formed by the decomposition of dimethyl sulfate. The mixture stirred in an ice bath for 5 min and then 6 M aqueous hydrochloric acid added until pH ~2–3 was reached whereupon a white precipitate formed. The solid was suction filtered through grade 1 filter paper and washed with ice-cold water (100 mL). Solid collected and dried under high vacuum overnight to give 1-methyl-4-oxo-1,4-dihydropyridine-3-carboxylic acid as a white solid, 46.19 g, 87% yield.

1H-NMR (400 MHz, DMSO-d6): δ 8.70 (s, 1H), 8.08 (d, J = 7.2 Hz, 1H), 6.76 (d, J = 7.2 Hz, 1H), 3.89 (s, 3H), −3.95 (br s, 0.24H)

**1-Methyl-4-oxo-1,4-dihydropyridine-3-carboxamide (4PY):** In a 1 L pear-shaped flask, N-methylmorpholine (21.1 mL, 192 mmol) was added to a stirred mixture of 1-methyl-4-oxo-1,4-dihydropyridine-3-carboxylic acid (22.58 g, 147.4 mmol) in dimethylformamide (DMF, 185 mL) to form a heterogeneous mixture. The resulting mixture stirred at room temperature for 10 min and then stirred at 0 °C in an ice bath for 20 min. Isobutyl chloroformate (23.0 mL, 177 mmol) was added over a period of 20 s whereupon the reaction mixture turned a yellow color. A large funnel was placed in the opening of the 1 L flask and Parafilm was used to seal the funnel to the glass joint to catch any potential overflow in case of vigorous bubbling of $CO_2$ after ammonium hydroxide addition. The resulting mixture stirred at 500 rpm for a total of 4 min at 0 °C and then the spin rate increased to 900 rpm and then a solution of chilled aqueous ammonium hydroxide (130 mL, 28–30%) and methanol (100 mL) (~0 °C chilled in an ice bath for 15 min) was added at once. The reaction mixture bubbled vigorously for ~5 s but did not overflow into the funnel. The resulting mixture stirred in the ice bath for 5 min and then at room temperature for 15 min. A small aliquot was taken and concentrated using high vacuum and 1H-NMR (DMSO-d6) of the concentrated aliquot showed primarily desired product and no starting material. The reaction mixture was stirred and treated with 6 M aqueous sodium hydroxide (29 mL, 174 mmol) at 0 °C to free base most of the ammonium chloride formed and then partially concentrated using rotary evaporation (full rotavap vacuum, 54 °C). Water (100 mL) was added and the mixture concentrated again on the rotavap to azeotrope most of the DMF. The mixture was then concentrated using high vacuum for 24 h to give a tan-yellow solid. The solid was dissolved in methanol (~300 mL) until white sodium chloride remained and the mixture suction filtered to remove sodium chloride. The methanol filtrate collected and concentrated using rotary evaporation and then high vacuum overnight. The resulting tan-yellow solid was triturated with dichloromethane (200 mL) and the solid along the walls of the flask were scraped into the dichloromethane and the large chunks were broken up with a spatula until a mostly fine solid remained. The resulting mixture swirled for 1 min and then

suction filtered to give an off-white solid which was rinsed with dichloromethane (100 mL). The solid air dried overnight to give 1-methyl-4-oxo-1,4-dihydropyridine-3-carboxamide (4PY) as an off-white solid, 22.17 g, 99% yield. 1H-NMR was consistent with previously reported 1H-NMR (Supplemental Figure 1).

1H-NMR (400 MHz, DMSO-d6) [72]: δ 9.58 (br s, 1H), 8.46 (s, 1H), 7.76 (d, J = 7.3 Hz, 1H), 7.44 (br s, 1H), 6.40 (d, J = 7.4 Hz), 3.78 (s, 3H)

HRMS: [M+H]+ calcd for $C_7H_9N_2O_2$, 153.0664 Da; found 153.0657 Da.

### N1-methyl-2-pyridone-5-carboxamide (2PY, IUPAC 1-methyl-6-oxo-1,6-dihydropyridine-3-carboxamide)

**1-methyl-6-oxo-1,6-dihydropyridine-3-carboxylic acid:** A mixture of 6-hydroxynicotinic acid (IUPAC 6-Oxo-1,6-dihydropyridine-3-carboxylic acid, 50.28 g, 361.4 mmol) and dimethyl sulfate was (120 mL, 1260 mmol) stirred at 100 °C (oil bath temperature) for 2.5 h. Afterwards, the reaction mixture was still a heterogeneous mixture suggesting that the dimethyl sulfate was not of good quality. A new bottle of dimethyl sulfate was then opened and used. Additional dimethyl sulfate (20 mL, 210 mmol) was added and the resulting mixture stirred at 100 °C for 30 min where it appeared that the heterogeneous reaction mixture was thinning out. Additional dimethyl sulfate (40 mL, 420 mmol) was added and the resulting mixture stirred at 100 °C whereupon the mixture clarified after 1 h. The mixture stirred an additional 45 min at 100 °C after clarifying and then cooled to room temperature with the assistance of an ice-water bath. 6 M Aqueous sodium hydroxide (360 mL) added slowly over a period of ~30 min until pH~12 was achieved. An ice bath was used to offset the exotherm resulting from the addition of sodium hydroxide solution. The addition was accompanied by the evolution of bubbles. The reaction mixture was then heated to 60 °C (internal temperature) and stirred for 10 min whereupon the bubbling slowed. Reaction mixture cooled to room temperature overnight. The reaction mixture was partially concentrated using rotary evaporation (10 bar, 40 °C water bath) to remove most of the liberated methanol (~90 mL). The reaction mixture was cooled in an ice bath and stirred and then acidified to pH~2–3 by adding 6 M aqueous HCl via a Pasteur pipette whereupon an off-white solid formed. The stirring rate was increased to 1150 rpm during HCl addition because the mixture became very thick. The resulting solid mixture suction filtered through filter paper (grade 1). The resulting solid was rinsed with water (200 mL) and then collected and dried under high vacuum for 48 h to give a light tan solid, 1-methyl-6-oxo-1,6-dihydropyridine-3-carboxylic acid, 53.85 g, 97% yield.

1H-NMR (400 MHz, DMSO-d6): δ 12.79 (br s, 1H), 8.48 (s, 1H), 7.78 (d, J = 9.4 Hz, 1H), 6.41 (d, J = 9.4 Hz, 1H), 3.50 (s, 3H)

**1-Methyl-6-oxo-1,6-dihydropyridine-3-carboxamide (2PY):** Triethylamine (20.3 mL, 146 mmol) was added to a mixture of 1-methyl-6-oxo-1,6-dihydropyridine-3-carboxylic acid (20.39 g, 133.1 mmol) in dichloromethane (180 mL) and the resulting mixture stirred at room temperature at 800 rpm until the solid had been incorporated into a translucent solution/suspension (~20 min). This solution/suspension was slowly poured into a stirred solution of thionyl chloride (10.6 mL, 146 mmol) in dichloromethane (100 mL) at 0 °C over

a period of ~4 min whereupon a dark tan precipitate formed. After addition, the resulting mixture was removed from the ice bath and stirred at room temperature for 20 min and then concentrated using rotary evaporation followed by high vacuum for 45 min to remove residual thionyl chloride. The flask containing the brown solid was placed in an ice bath and then treated with a chilled (ice bath) solution of aqueous ammonium hydroxide (160 mL, ~1280 mmol) in methanol (100 mL) at once. The resulting mixture stirred at 700 rpm at 0 °C for 10 min and then at room temperature for 30 min. The very cloudy mixture was treated with 6 M aq sodium hydroxide (45 mL, 270 mmol) to freebase the ammonium chloride and triethylamine hydrochloride. The mixture was concentrated using rotary evaporation and then high vacuum for 5 h to give a brown solid. The solid was treated with methanol (750 mL) and the resulting mixture heated to ~45 °C and swirled for 5 min leaving behind a white solid (sodium chloride) and a small amount of a light brown solid. The mixture was suction filtered through a pad of Celite and the clear brown filtrate collected and concentrated using rotary evaporation to give a brown solid. The solid was washed with methanol (150 mL) by swirling for 5 min and then sat for 1 h. The brown methanol layer above the solid was decanted off leaving the tan solid behind and then fresh methanol (100 mL) added to the solid. The mixture swirled for 5 min and then suction filtered through grade 1 filter paper to give a light tan solid that was dried under high vacuum for 3 h to give 1-methyl-6-oxo-1,6-dihydropyridine-3-carboxamide (2PY), 21.47 g, >100% yield (106%). 1H-NMR was consistent with previously reported 1H-NMR (Supplemental Figure 2).

1H-NMR (400 MHz, DMSO-d6) [73]: δ 8.42 (s, 1H), 7.87 (d, J = 9.4 Hz, 1H), 7.76 (br s, 1H), 7.24 (br s, 1H), 6.39 (d, J = 9.4 Hz, 1H), 3.47 (s, 3H)

HRMS: [M+H]+ calcd for $C_7H_9N_2O_2$, 153.0664 Da; found 153.0663 Da.

### Targeted LC/MS/MS Analysis of Human Serum Samples

Stable-isotope-dilution LC/MS/MS was used for quantitation of 2PY and 4PY in human and mouse serum. Four volumes of ice-cold methanol containing internal standard (d3–2PY, d3–4PY) was added to serum samples, followed by centrifugation (21,000 × g; 4°C for 15 min). The clear supernatant was transferred to glass vials with microinserts and LC/MS/MS analysis was performed on a chromatographic system consisting of two Shimadzu LC-30 AD pumps (Nexera X2), a CTO 20AC oven operating at 40°C, and a SIL-30 AC-MP autosampler in tandem with a 8050 triple quadruple mass spectrometer (Shimadzu Scientific Instruments, Columbia, MD, USA). For chromatographic separation (Extended Data Figure 4), a HILIC column (100 mm × 2.1 mm; 2.6 μm) (Cat # 00D-4461-AN, Phenomenex, Torrance, CA) was used. The mobile phases consisted of A (5 mM ammonium acetate, 0.1% acetic acid in water) and B (5mM ammonium acetate, 5% water, 0.1% acetic acid in acetonitrile). The separation was conducted using the following gradient: 0 min 100% B; 0–1.5 min 100% B; 1.5–4 min 100–25% B; 4–6 min 25% B. After analysis, the column was washed with two cycles of 100% B for 1 min, then 10% B for 1 min, then equilibrated with 100% B for 1 min before the next sample injection. A sample volume of 1 μL was used for the injection. Sample temperature was maintained at 4°C.

Electrospray ionization in positive mode with multiple reaction monitoring (MRM) was used with the following transitions: *m/z* 153 → 110 for 2PY, *m/z* 153 → 136 for 4PY, *m/z* 156

→ 113 for d3–2PY, *m/z* 156 → 139 for d3–4PY. The following ion source parameters were applied: nebulizing gas flow, 3 L/min; heating gas flow, 10 L/min; interface temperature, 300°C; desolvation line temperature, 250°C; heat block temperature, 400°C; and drying gas flow, 10 L/min. The limit of detection (LOD; 3:1 signal to noise cutoff) was 0.53 μM for 2PY and 0.01 μM for 4PY. The limit of quantification (LOQ; 10:1 signal to noise cutoff) was 1.34 μM for 2PY and 0.04 μM for 4PY. For samples with signal to noise ratio <3, concentrations were reported as one half of the LOD, and samples with signal to noise ratio ≥3 and <10 were reported as one half of the LOQ. Quality control samples were run with each batch of samples and inter-batch variations expressed as coefficient of variation (CV) were less than 15% for 2PY and less than 10% for 4PY. For data analysis, the software Lab Solutions (Shimadzu) was used.

## Genotyping and Imputation

The US Validation cohort (n = 2,331) was selected from among GeneBank subjects who had previously been genotyped with either the Affymetrix Genome-Wide Human Array 6.0 Chip (n=3,031) or the Illumina Infinium Global Screening Array-24 v2.0 (GSA) BeadChip (n=1,728) [17]. Prior to imputation, genomic coordinates of SNPs on each genotyping platform were first converted to GRCh37/hg19. Quality control steps included removal of duplicate SNPs as well as those with call rates <97%, minor allele frequencies (MAFs) <1%, and without chromosome and base pair position. Individuals with genotype call rates <90%, of African American ancestry, and outliers from PCA analysis were also excluded, resulting in 671,968 SNPs in 2,972 participants genotyped with the Affymetrix 6.0 Chip, and 539,533 SNPs in 1,624 participants genotyped with the GSA Chip. Imputation was carried out for unmeasured SNPs on the forward (+) strand using 1000 Genomes Project (Phase 3 release, v5) and Haplotype Reference Consortium (vr1.1 2016) as reference panels through the University of Michigan Imputation Server (https://imputationserver.sph.umich.edu). After imputation, subjects with discordant sex were excluded and SNPs that had Hardy-Weinberg equilibrium P-values <0.0001, were duplicates or multiallelic, had imputation quality scores <0.3, and with MAFs <1% were removed. This resulted in 9,225,856 autosomal SNPs included in the GWAS analyses.

## Genome-wide Association Studies (GWAS) and Meta-analyses

Serum 2PY and 4PY concentrations in the US Validation Cohort were natural log transformed and used for genome wide association studies (GWAS) using linear regression analysis assuming an additive model with adjustment for age, sex, and genotyping array, as implemented in Plink v1.9 [74]. Z-score-based meta-analyses with sample-size weighting were conducted for both metabolites combining GWAS results obtained in the US Validation Cohort with publicly available summary statistics using METAL [75,76] (Supplemental Table 1). The genomic control factor (λ) was used to evaluate population stratification and the genome-wide significance threshold for analyses of 2PY and 4PY was set at $P=5\times10^{-8}$. Manhattan and regional plots were generated using the ‘qqman’ package (v0.1.4) and LDproxy tool (https://ldlink.nci.nih.gov/), respectively. Phenome-wide association study (PheWAS) analysis of identified variants for association with other traits was performed using previously published proteomic and metabolomic GWAS datasets [24,53].

## Expression Quantitative Trait Locus Analysis

Meta-analysis combining our GWAS results in the US Validation Cohort with publicly available summary statistics revealed the genetic variant rs10496731, which maps to the gene encoding aminocarboxymuconate semialdehyde decarboxylase (*ACMSD*), is associated with serum levels of 2PY and 4PY (Extended Data Table 1). Since the enzyme ACMSD regulates nicotinamide adenine dinucleotide (NAD) synthesis from tryptophan (Figures 1,6), we speculated the genetic variant rs10496731 impacts 2PY and 4PY synthesis by regulating ACMSD function. We tested this hypothesis by searching for tissue-specific expression quantitative trait loci (eQTLs) reported in the Genotype Tissue Expression (GTEx) Project for rs10496731. GTEx performed RNA sequencing on 47 human tissues, and two appreciably expressed mRNA splice variants coding for ACMSD were expressed in liver and kidney [23]. Although no eQTLs were reported in those tissues, rs10496731 was yielded a splice QTL (sQTL) for *ACMSD* in liver (n=208, $P=1.3\times10^{-7}$, Figure 4d), where genotype was associated with differential abundance of two mRNA isoforms.

Previous studies [77] had tested enzymatic activity of the two *ACMSD* splice variants, one of which was functional (ENST00000356140) and exhibited aminocarboxymuconate semialdehyde consumption activity while the other, nonfunctional, isoform (ENST00000392928) demonstrated no such activity. Moreover, critical residues demonstrated by site-directed mutagenesis were found to be encoded by exon 2, which is present in the functional mRNA isoform but spliced out of the nonfunctional isoform.

The genetic variant associated with increased 2PY and 4PY levels, rs10496731, was associated with increased retention of the second exon of *ACMSD* pre-mRNA [23]. Since excision of exon 2 is required to form a functional ACMSD enzyme [77], the T allele of rs10496731 would thus lead to decreased ACMSD activity and shunting of ACMS towards production of quinolinate, nicotinamide metabolites, and, ultimately, 2PY and 4PY (Extended Data Figure 2). Consistent with this model, the T allele of rs10496731 was also significantly associated with increased levels of both quinolinate and 1-methylnicotinamide [53] (Supplemental Table 7). Together with our animal studies showing *Acmsd* knockdown increases 2PY and 4PY serum levels (Figure 4g), these data suggest the genetic variant rs10496731 regulates 2PY and 4PY synthesis via differential splicing of *ACMSD* pre-mRNA.

## Genetic Analyses in the UK Biobank

Primary level data from the UK Biobank were used to carry out genetic analyses with the lead variant identified for 2PY and 4PY. Briefly, the UK Biobank recruited a total of 503,325 participants between 2006–2010 who were 40–69 years of age and registered with a general practitioner of the UK National Health Service [78]. At enrollment, extensive data on demographics, medication use, and disease-related outcomes were obtained through questionnaires and health records. Baseline blood samples were also collected for measurement of serum biomarkers that are either established disease risk factors or routinely measured as part of clinical evaluations. Quality control of samples, genotyping, and imputation of ~90 million SNPs in the UK Biobank were performed by the Wellcome Centre for Human Genetics, as described previously [78]. Proteomics measurements (~1400

targets) based on the Olink Explore 1536 platform were also recently made available in a subset of 54,306 participants [28]. These data were used to test rs10496731 for association with serum sVCAM-1 levels (n=51,285) by linear regression analysis, with adjustment for age, sex, the first 10 principal components (PC1–10), and genotyping array. A meta-analysis was carried out with results in the UK Biobank for rs10496731 with publicly available summary statistics for sVCAM-1 levels using a Z-score approach, as described above for 2PY and 4PY.

Cox proportional hazards models were used to assess association of rs10496731 with incident major adverse cardiac events (MACE=MI, stroke, or death) in UK Biobank from the date of enrollment up to 5,000 days of follow-up. MI was defined based on International Classification of Diseases version-10 (ICD10) code I21, I22, I23, I25.2, as well as doctor-diagnosed and self-reported MI, as described previously [30]. Similarly, stroke was defined based on ICD10 codes I63 and I64, as well as doctor-diagnosed and self-reported stroke. Participants who experienced a MACE within the first 14 days were excluded and all analyses were adjusted for age at the time of ICD-10 code assignment, sex, PC1–10, genotyping array, education, diabetes, asthma, smoking, lipid medication use, and anti-hypertension medication use.

## Mendelian Randomization (MR) Analyses

To evaluate whether 2PY and 4PY levels were causally associated with CVD outcomes, we carried out MR analyses with the Wald ratio method, as implemented in the Two-Sample MR package in R v4.0.3 [54]. The genetic instrument for the exposures were based on the effect sizes of rs10496731 on 2PY and 4PY levels obtained from the meta-analyses. For the outcomes, effect estimates were derived from our analysis of rs10496731 with risk of incident MACE in the UK Biobank, as well as those from publicly available summary statistics for CAD [29], MI [30], and stroke [31]. Power calculations for Mendelian Randomization studies were performed based on a method developed for estimating power with single instrumental variables [79].

## Adeno-associated virus (AAV) Knockdown Studies

Short hairpin RNA (shRNA) coding sequences targeting *Acmsd,* or a scrambled version, were synthesized by VectorBuilder (Burlingame, CA) and cloned into a single-strand AAV vector and expression driven by a U6 promoter to make pAAV-shRNA_EGFP-T2A-Bsd-U6_mAcmsd Scramble[shRNA#1] (control) and pAAV-shRNA_EGFP-T2A-Bsd-U6>mAcmsd[shRNA#1] (knock-down), respectively. Sequences and maps are available at https://doi.org/10.5281/zenodo.8357441. Recombinant *Acmsd* and scrambled shRNA encoding vectors were transfected into AAV8 serotype packaging cells by VectorBuilder and concentrated purified AAV's were obtained for each construct. Validation of knock-down of *Acmsd in vivo* was performed as described below.

## Acmsd Knockdown in Mice

All animal procedures were approved by the Institutional Animal Care and Use Committee. Experiments were designed to minimize distress and the number of animals used. Experiments were conducted on 12 week old female C57Bl/6 mice (purchased from Jackson

Laboratories, Bar Harbor, ME, USA). Animals were maintained under a strict 14 h light/10 h dark cycle with water and food available ad libitum and temperature of 20–26 °C and 30–70% humidity. All mice were given access to chow and water *ad libitum*. AAVs were designed to express shRNA with a randomized targeting sequence (referred to hereafter as scrambled or control) or a sequence targeting *Acmsd* mRNA transcripts (referred to hereafter as knockdown) as described above. Mice were injected intravenously via tail vein with either scrambled or knockdown AAV (1 mL, $1\times10^{11}$ gc) in sterile, physiological (0.9% wt/v) saline. Serum was serially monitored over time for 2PY and 4PY levels, and after noting significant increase (after 4 weeks), both serum and tissues were collected for analysis.

## Cell Culture

Second-passage human umbilical vascular endothelial cells (HUVECs) were graciously provided by the Fox group (Cleveland, OH). HUVECs were expanded in EGM-2 media (Cat. # CC-3162, Lonza, Basel, Switzerland) to passage four and seeded overnight in full media. HUVECs were then serum starved for three hours in EBM-2 media (Cat. # CC3156, Lonza) and exposed to metabolites or lipopolysaccharide (LPS) in EBM-2 with 1.5% fetal bovine serum. RNA was collected after four hours of exposure, and in separate experiments with HUVEC cells, protein was collected after six hours of exposure.

## Immunohistochemistry

Mouse aortas were collected after six hours of exposure to 2PY, 4PY, or vehicle control (saline), and stained for VCAM-1 for protein quantification or PECAM (CD31) to confirm the position of the endothelium. Frozen sections of aortas were mounted on glass slides, fixed with IC fixation buffer (Cat. # 00–8222-49 Invitrogen, Carlsbad, CA) for 20 min, and washed twice in deionized water. After quenching endogenous peroxidase with 3% hydrogen peroxide (Cat. # H325–100, Fisher Chemical) for 10 min, non-specific avidin-biotin activity was blocked with an avidin/biotin blocking kit (Cat. #SP-2001, Vector laboratories, Burlingame, CA). Sections were then blocked with normal rabbit serum Blocking Reagent (Catalogue # S-5000, Vector laboratories, Burlingame, CA) for 1 h followed by overnight incubation with the primary antibodies: rat anti-mouse VCAM1 (CD106) (Cat. # 550547, 0.625 μg/mL BD Pharmingen, San Diego, CA), goat anti-mouse PECAM (CD31) (Cat # AF3628, 15ug/mL, R&D Systems, Minneapolis, MN). The slides were developed by Vectastain Elite ABC (Cat. # PK-6105, Vector laboratories, Burlingame, CA) with 3-amino-9-ethylcarbazole (AEC, Cat. # K3464, Dako, Jena, Germany) and then counterstained with hematoxylin (Cat. # H-3401, Vector laboratories, Burlingame, CA) and mounted in Aqua-Poly/Mount medium (Cat. # NC9439247, Polysciences, Warrington, PA). Images were taken using a wide-field slide scanner at 20X magnification. Quantification was performed using the software QuPath v0.3.0. Background values were adjusted once for each sample by measuring average background within each image to minimize error due to minor intensity variations across the image set. AEC signal was isolated using the color deconvolution function of QuPath. Using three manually annotated tissue sections separate from those used for protein quantification, a random forest classifier was trained to classify pixels as high, medium, low, or absent of AEC signal. The pixel classifier was then used to classify pixels within three high-magnification fields from each experimental tissue sample.

Pixel-H-scores [80] were then calculated for three high-magnification fields from each sample and the mean score was reported. Pixel-H-scores were calculated as:

$$H = 100\frac{3H + 2M + L}{H + M + L + A}$$

where H, M, L, and A refer to the number of pixels classified as high, medium, low, and absent respectively.

## Intravital Microscopy

Mice were injected intraperitoneally with 10mg/kg 4PY, 2PY, or vehicle control (saline) at 0, 2 and 4 hours (the amount injected was selected after establishing peak plasma levels of 4PY and 2PY observed are within the range of concentrations observed in the 4$^{th}$ quartile of the US Validation Cohort). Intravital microscopy was conducted at the six-hour time point. To visualize leukocyte adhesion within auricular venules, mice were anesthetized with 100 mg/kg ketamine and 10 mg/kg xylazine. Leukocytes were labeled with jugular vein injections of 0.1 mL of rhodamine 6G (4 mg / mL). Mice were placed in a supine position in a 15 cm dish with ears flat on the dish. 50 μL of deionized water was placed on the surface of the ear, and an intravital microscope equipped with an immersion lens and video camera was used to visualize labeled cells.

For each animal, three unbranched segments of auricular venules with a diameter 30 – 150 μm and approximate length of 300 μm were recorded for 5 min each. Mice were then euthanized after collection of blood via cardiac puncture. The recorded videos were analyzed using Stream Pix (v7.3.0.0), as previously described [81] by investigators blinded to animal group. Leukocyte adhesion was defined as those leukocytes firmly adherent to the vessel wall for ≥ 30 sec. Firmly adherent leukocytes were counted and normalized to the area of the counted vessel region to correct for differences in vessel size.

## Real-time quantitative PCR

Total RNA was isolated from tissues or cells using a TRIZOL RNA isolation protocol (Cat. # 15–596-018, Fisher, Waltham, MA). Reverse transcription was performed using a High-Capacity RNA to cDNA kit (Cat. # 4387406, Applied Biosystems, Foster City, CA). Real time (RT) quantitative PCR was carried out following the TaqMan Gene Expression Assays protocol using the recommended RT primers and probes of mouse *Acmsd* (Cat # 4331182, Applied Biosystems) and primer-limited mouse *Gapdh* (Cat # 4331182, Applied Biosystems) or human *VCAM1* (Cat # 4331182, Applied Biosystems) and primer limited human *GAPDH* (Cat # 4331182, Applied Biosystems).

## Western Blotting

Tissues or cells were lysed in radio-immunoprecipitation assay (RIPA) cell lysis buffer (Cat # 9806S, Cell Signaling, Danvers, MA) containing a protease/phosphatase inhibitor cocktail (Catalogue # 5872, Cell Signaling). Total protein was quantified with a bicinchoninic acid (BCA) protein assay kit (Catalogue # 23225, ThermoFisher, Waltham, MA). The following antibodies were used for detection of mouse ACMSD: rabbit anti-mouse ACMSD (Cat. #

PA5–90853, 0.7 μg/mL, Invitrogen), rabbit anti-mouse Tubulin (Cat. # 2148, 0.05 μg/mL, Cell Signaling), 680RD goat anti-rabbit IgG (Cat. # 926–68071, 0.1 μg/mL, LiCor Inc, Lincoln, NE), 800CW goat anti-rabbit IgG (Cat. # 926–32211, 0.1 μg/mL, LiCor Inc). The following antibodies were used for detection of human VCAM-1: rabbit anti-human VCAM-1 (Cat. # 13662, 0.6 μg/mL, Cell Signaling, Danvers, MA), mouse anti-human GAPDH (Cat. # MA5–15738, 0.6 μg/mL, Invitrogen, Waltham, MA), 680RD goat anti-rabbit IgG (Catalogue # 926–68071, 0.1 μg/mL, LiCor Inc, Lincoln, NE), 800CW goat anti-mouse IgG (Catalogue # 926–32210, 0.1 μg/mL, LiCor Inc, Lincoln, NE. Band intensity was scanned using the Odyssey Imaging System (LiCor Inc). The software ImageStudio (v5.2) was used to quantify images.

## Statistics

Sample distributions were tested for normality with the Shapiro-Wilks test, and distributions with $P > 0.1$ were considered normal. Normally distributed groups were compared with one-way ANOVA with post-hoc student t tests. For non-normally distributed groups, Wilcoxon rank sum tests were used to compare between-group differences. Kruskal-Wallis test with post-hoc Dunn's test was used to compare multiple groups. Trend tests (Jonckheere-Terpstra) were used to test for ordered differences among 2PY and 4PY quartiles or genotypes.

Kaplan-Meier analysis was used for time-to-event analysis of outcomes. For analyses, all subjects, both MACE and non-MACE, had similar follow-up (3yr) time. Risk differences among quartiles were assessed with the log-rank test. Cox proportional hazards regression was used to assess the independence of metabolite associations. Cox models for the US and European Validation Cohorts included covariates for metabolite quartile, age, sex, systolic blood pressure, low density lipoprotein cholesterol (LDL), high density lipoprotein cholesterol (HDL), triglycerides (or dyslipidemia for European Validation Cohort, as indicated below), diabetes status, high-sensitivity C-reactive protein (hsCRP), current (active) smoking status, alcohol use. The US Validation Cohort was additionally adjusted for education level. Because approximately 30% of lipid profiles were incomplete in the European Validation Cohort (missing triglyceride levels), adjustment for dyslipidemia status was substituted for LDL, HDL, and triglyceride values for this cohort. Dyslipidemia was defined as LDL ≥ 100 mg/dL, or HDL ≤ 40 mg/dL for males or HDL ≤ 50 mg/dL for females, or triglycerides ≥ 150 mg/dL (where available). All statistical analyses were performed using R version 4.2.2 (R Foundation for Statistical Computing, Vienna, Austria). Kaplan-Meier and Cox proportional hazards analysis were performed with the survival package version 3.1–12.

For boxplots, the central line represents the median while the upper and lower hinges represent the interquartile range. The lower whisker represents the smallest observation greater than or equal to the lower hinge minus 1.5 times the interquartile range. The upper whisker represents the largest observation less than or equal to the upper hinge plus 1.5 times the interquartile range. All reported P values are two-sided. P values are adjusted to a false discovery rate of 0.05 where indicated. A P value < 0.05 was considered statistically significant.

## RNA Sequencing

HUVECs were incubated with vehicle as a negative control, 2PY (100μM), 4PY (100μM), or LPS as a positive control for 4 hours and total RNA was isolated using a TRIZOL RNA isolation protocol (Cat. # 15–596-018, Fisher, Waltham, MA). For all samples, RNA was quantitated using a Qubit RNA HS Assay kit (Cat# Q32852, Invitrogen, Waltham, MA) and Qubit fluorometer (Cat# 33238, Invrogen, Waltham, MA) according to the manufacturer's instructions. The RNA integrity number (RIN) for each sample was measured using an Agilent 2200 TapeStation. RNA-seq libraries were generated using Illumina Total RNA Prep with Ribo-Zero Plus (Cat. # 20040525, Illumina, San Diego, CA). Sequencing libraries were sequenced on the NovaSeq 6000 System at the Microbial Sequencing & Analytics Resource facility at the Lerner Research Institute. Reads were trimmed of low-quality reads and adapter sequences using Trimmomatic (v0.32) [82]. Quality filtered reads were mapped to the human genome (version GRCh38.p14), using STAR (v020201) [83]. Transcripts per million (TPM) and expected counts for each gene were calculated using RNAnorm (https://github.com/Lyd0527/RNAnorm). Differential expression analysis was conducted using the Bioconductor package edgeR (v3.22.3) [84] using the decideTestsDGE function. The differentially expressed gene lists can be found in Source Data. Functional enrichments of gene ontology (GO) categories were performed using the package topGO (v1.0) [85] in R.

## Extended Data

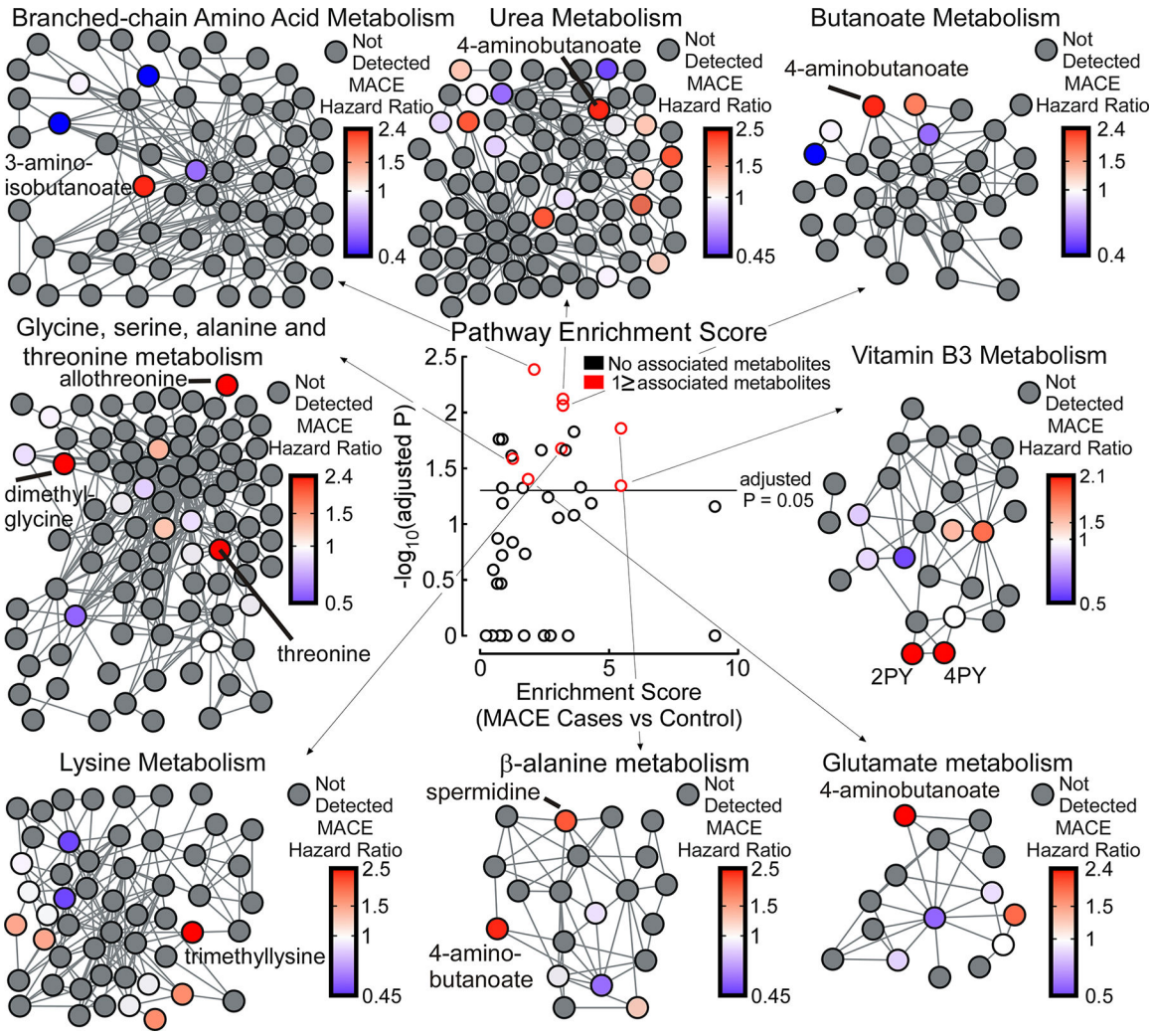


**Extended Data Fig. 1. Network module-based pathway analysis identifies MACE-associated pathways containing MACE-associated metabolites**

(**center scatterplot**) MACE-associated metabolite enrichment scores versus enrichment P values for metabolic pathways (each point represents a pathway) defined in the Human MFN genome-scale metabolic model, as released with Metaboanalyst v4.0 (Supplemental Methods). Previously, Human MFN was constructed as a network by defining all human metabolites listed in KEGG (release 81.0), SMPDB v2.0, HMDB v4.0, ChEBI (release 131), and Biocyc (release 17.0) as points (nodes) and all chemical reactions (enzymatic or otherwise) as connections (edges) between metabolites (Supplemental Methods). Thus, any two molecules (nodes) participating in the same enzymatic reaction are connected with a line (edge). Metabolites (nodes) are separated into pathways (modules) to maximize the ratio of within-group to between-group connections. Pathway enrichment scores (ratio of observed to expected MACE-associated metabolites) and enrichment P values were determined with mummichog (v1.0.10), as implemented in Metaboanalyst v4.0 (Supplemental Methods), which includes adjustment for multiple testing. In the center

scatterplot, each point represents the enrichment score (ratio of observed to expected MACEassociated metabolites) and the P value for the pathway (module). Each pathway (module) with enrichment P value < 0.05 and at least one component metabolite (node) with prospective 3-year MACE hazard ratio (highest vs lowest quartile) P < 0.005 is highlighted in red. P values for all metabolites and pathways are shown in Supplemental Table 5. (**outer modules**) Shown are nine pathways (network modules) that were enriched with MACE-associated metabolites (enrichment P values < 0.05) and contained at least one component metabolite associated with prospective 3-year MACE (hazard ratio P < 0.005, two-sided Wald test assuming a univariate Cox model with no adjustment for multiple testing). Spectral features detected during untargeted metabolomics analysis were assigned to any molecule with a predicted massto-charge ratio within measurement error of the observed *m/z*, producing multiple assignments per feature (Supplemental Methods). Names of each network modulebased pathway are shown, and within each pathway, lines (edges) indicate a shared metabolic conversion between the two connected metabolites (nodes), and metabolites (nodes) are colored according to the magnitude of the prospective 3- year MACE hazard ratio. Note that the "Vitamin B3 Metabolism" (niacin/NAD metabolism) pathway module was enriched with MACE-associated metabolites (enrichment P = 0.048) and the top unidentified metabolite (by incident MACE risk hazard ratio), with *m/z* = 153.0656 Da was assigned to both 2PY and 4PY within the "Vitamin B3 Metabolism" pathway module.

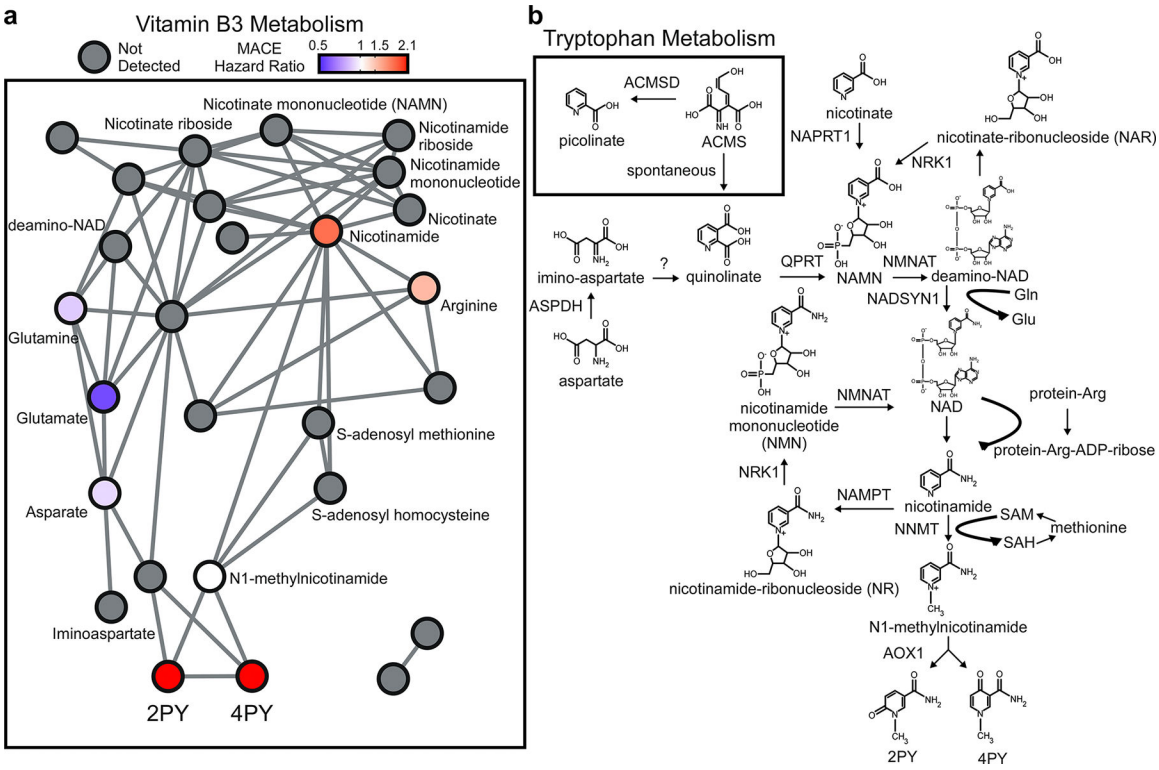


**Extended Data Fig. 2. Overview of vitamin B3 metabolism, as defined in the Human MetaFishNet (MFN) model**

(**a**) Network module for vitamin B3 (niacin/NAD) metabolism. Previously, Human MFN was constructed as a network by defining all human metabolites listed in KEGG (release 81.0) SMPDB v2.0, HMDB v4.0, ChEBI (release 131) and Biocyc (release 17.0) as points (nodes) and all chemical reactions (enzymatic or otherwise) as connections (edges) between metabolites (Supplemental Methods). Thus, any two molecules (nodes) participating in the same enzymatic reaction are connected with a line (edge). Metabolites (nodes) are separated into pathways (modules) to maximize the ratio of within-group to between-group connections. Pathway enrichment P values (MACE cases vs controls) were determined with mummichog (v1.0.10), as implemented in Metaboanalyst v4.0 (Supplemental Methods), which includes adjustment for multiple testing. The vitamin B3 network module was enriched with MACE-associated metabolites (enrichment P=0.048), and a mass spectral feature (*m/z* = 153.0656 Da) assigned to metabolites (nodes) 2PY and 4PY was associated with prospective 3-year MACE risk (highest vs lowest quartile, unadjusted hazard ratio (HR) [95% confidence interval (CI)]=2.77[1.59–4.86], P=0.005[two-sided Wald test, no adjusted for multiple testing]). Further CVD risk analysis of this mass spectral feature is shown in Figure 2a–b. Metabolite (node) colors indicate the MACE hazard ratio (highest vs lowest quartile), while grey indicates the metabolite was not detected. Edges indicate a shared metabolic conversion between the two connected metabolites. Cofactors are not labeled. P values for all metabolites and pathways are shown in Supplemental Table 5. (**b**) Pathway representation of vitamin B3 metabolism using the molecules and reactions defined in the Human MFN model. The conversion of iminoaspartate to quinolinate was inferred in Human MFN, and so no enzyme is listed. NAD, nicotinamide adenine dinucleotide; ACMS, aminocarboxymuconoate semialdehyde; NAMN, nicotinic acid mononucleotide; SAM Sadenosyl methionine; SAH, S-adenosyl homocysteine.

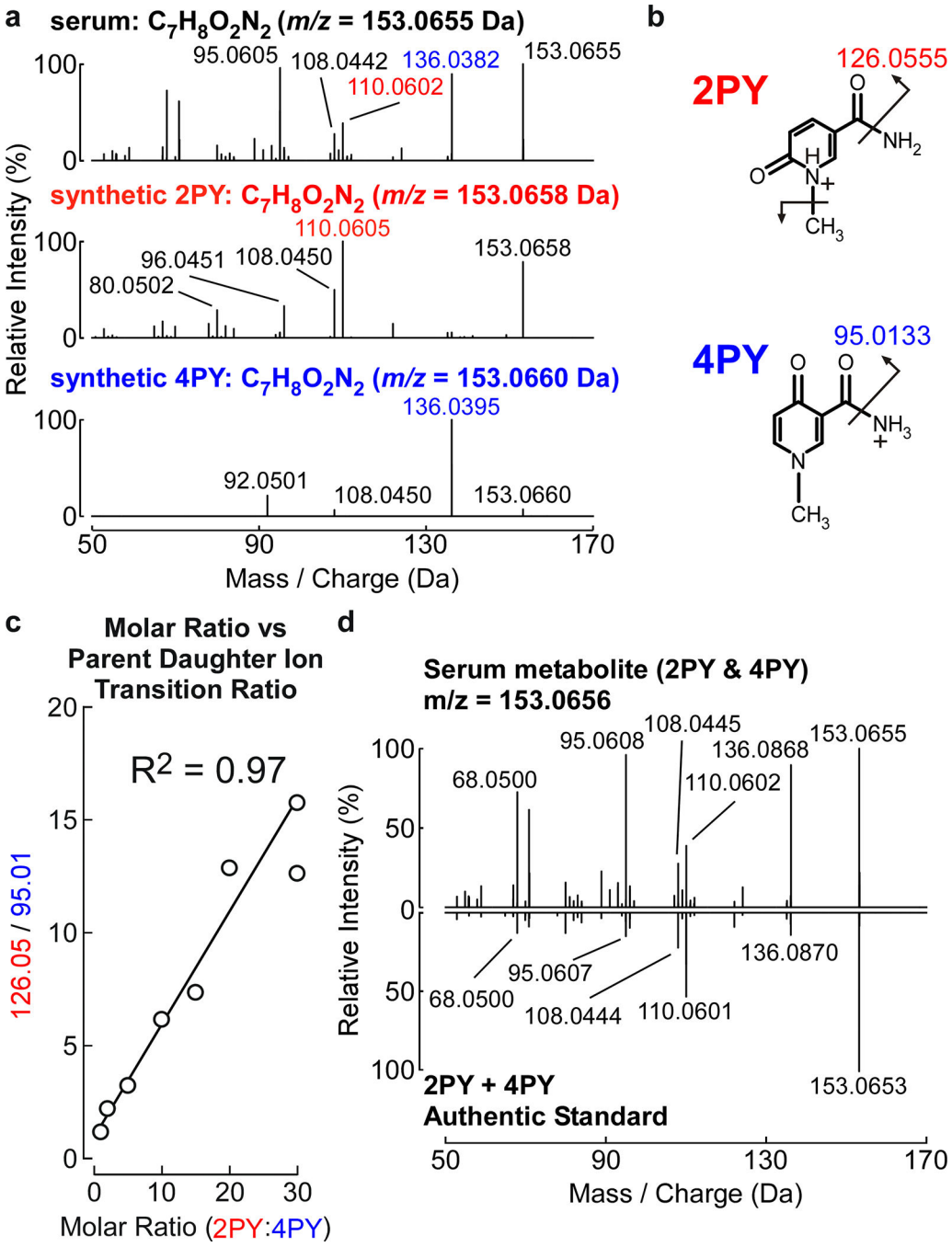


**Extended Data Fig. 3. Serum metabolite (m/z = 153.0656 Da) produces CID spectrum similar to a mixture of synthetic 2PY and 4PY**

Untargeted metabolomics revealed a serum analyte (*m/z* = 153.0656 Da) associated with prospective residual MACE risk. Network module-based pathway analysis suggested this serum analyte (*m/z* = 153.0656 Da) was a mixture of the structural isomers 2PY and 4PY, which have the same elemental composition (Supplemental Methods). As the collision-induced dissociation (CID) mass spectrum of the MACE-associated serum analyte (*m/z* = 153.0656 Da) included characteristic daughter ions of both 2PY and 4PY, we explored whether a mixture of synthetic 2PY and 4PY could reproduce the CID mass spectrum of

the serum analyte before conducting further structural studies and developing a method of independently quantitating 2PY and 4PY. Chemical synthesis of 2PY and 4PY is described in Supplemental Methods, and 1H-NMR spectra of synthetic material are shown in Supplemental Figures 1 and 2. (**a**) Comparison of the high-resolution collision-induced dissociation (CID) mass spectra in positive ion mode of the unknown MACE-associated serum analyte with *m/z* = 153.0656 Da and calculated elemental formula $C_7H_8O_2N_2$ (top), with synthetic 2PY (middle) and 4PY (bottom). 2PY and 4PY both have the elemental formula $C_7H_8O_2N_2$, and their observed *m/z* values are within measurement error (5 ppm) of 153.0656 Da. A CID parent-to-daughter transition characteristic, but not unique to 2PY (*m/z* = 110.0605 Da) is shown in red while a CID transition characteristic to 4PY (*m/z* = 136.0395 Da) is shown in blue. The spectrum of the serum analyte (top) contained parent-to-daughter transitions characteristic of 2PY and 4PY. (**b**) Parent-to-daughter transitions that are predicted to be unique to 2PY (*m/z* = 126.0555 Da) and 4PY (*m/z* = 95.0133 Da). These unique daughter fragments are detected at very low intensities as shown in Source Data. (**c**) We hypothesized the serum analyte with *m/z* = 153.0656 Da was a mixture of 2PY and 4PY. Without the capability to chromatographically separate 2PY and 4PY and compare to pure authentic chemical standards, we estimated the molar ratio of 2PY and 4PY in human serum in order to compare the presumed mixture to an equivalent mixture of 2PY and 4PY chemical standards. The molar ratio of 2PY:4PY in solution can be calibrated with the ratio of unique predicted parent-to-daughter transition intensities. The calibration curve prepared using 2PY and 4PY chemical standards in deionized water is shown. This molar ratio calibration curve was only used for exploratory structural studies and does not estimate absolute concentrations of 2PY and 4PY. Later, different calibration curves were used for independent quantitation of 2PY and 4PY using chromatographic separation. (**d**) Comparison of CID spectra of serum analyte with *m/z* = 153.0656 Da (top) with a solution of 2PY and 4PY in deionized water at the estimated molar ratio.

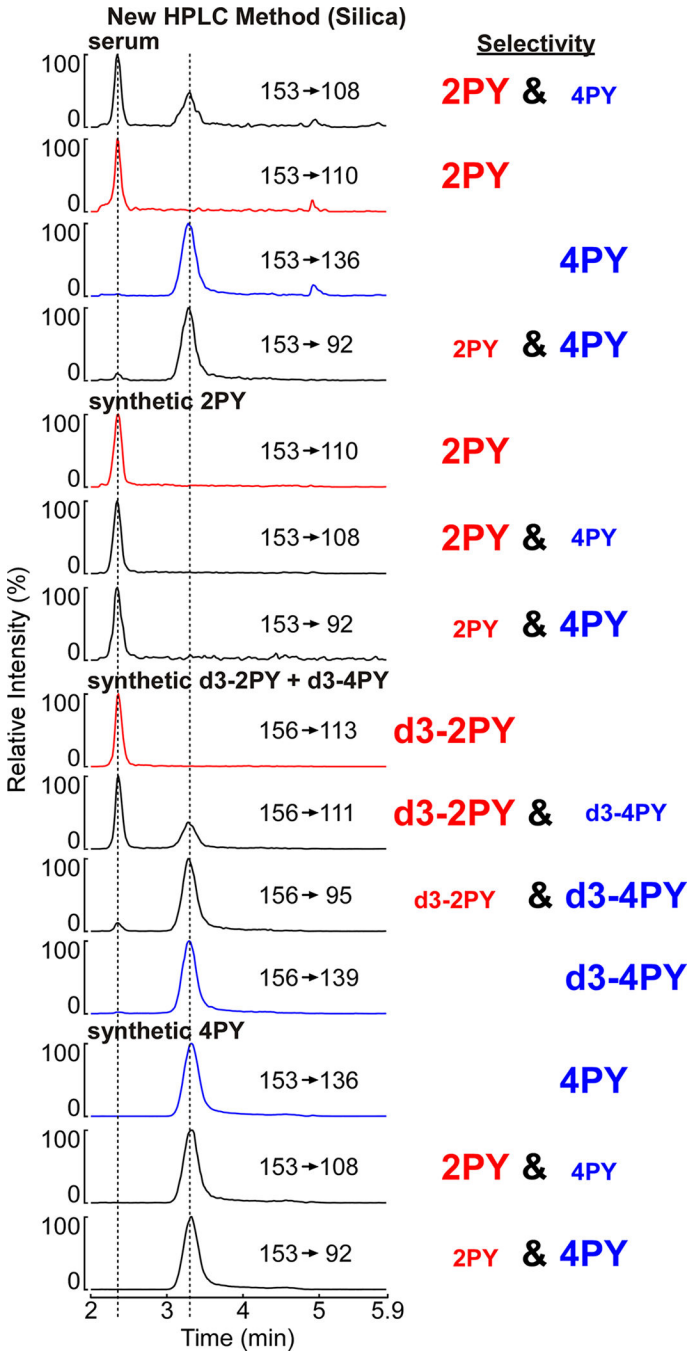


**Extended Data Fig. 4. Illustration of methods development to selectively monitor and quantify serum levels of 2PY and 4PY**

Shown is the baseline chromatographic resolution of 2PY and 4PY in serum, coupled with the selective MRM transitions used to quantify 2PY and 4PY. Briefly, isotope labeled synthetic 2PY and 4PY (d3–2PY and d3–4PY) were added to serum samples, protein precipitated with methanol, and then following injection on silica column, the indicated isotopologues of 2PY and 4PY were resolved and monitored by the indicated MRM transitions. The selectivity of the MRM transitions for either 2PY (red) or 4PY (blue) are indicated, with change in font size used to indicate selectivity for either 2PY or 4PY

(or their corresponding d3-isotopologue internal standards). Chemical synthesis of 2PY and 4PY is described in Supplemental Methods, and 1H-NMR of synthetic material are shown in Supplemental Figures 1 and 2. Note that the three distinct MRM transitions selected for monitoring natural abundance 2PY, 4PY, and their heavy isotope-labeled are also shown. The selected MRM transitions are also shown in Figure 2d. Note how the silica column-based method baseline resolves 2PY and 4PY within the MACE-associated serum analyte with *m/z* = 153.0656 Da.

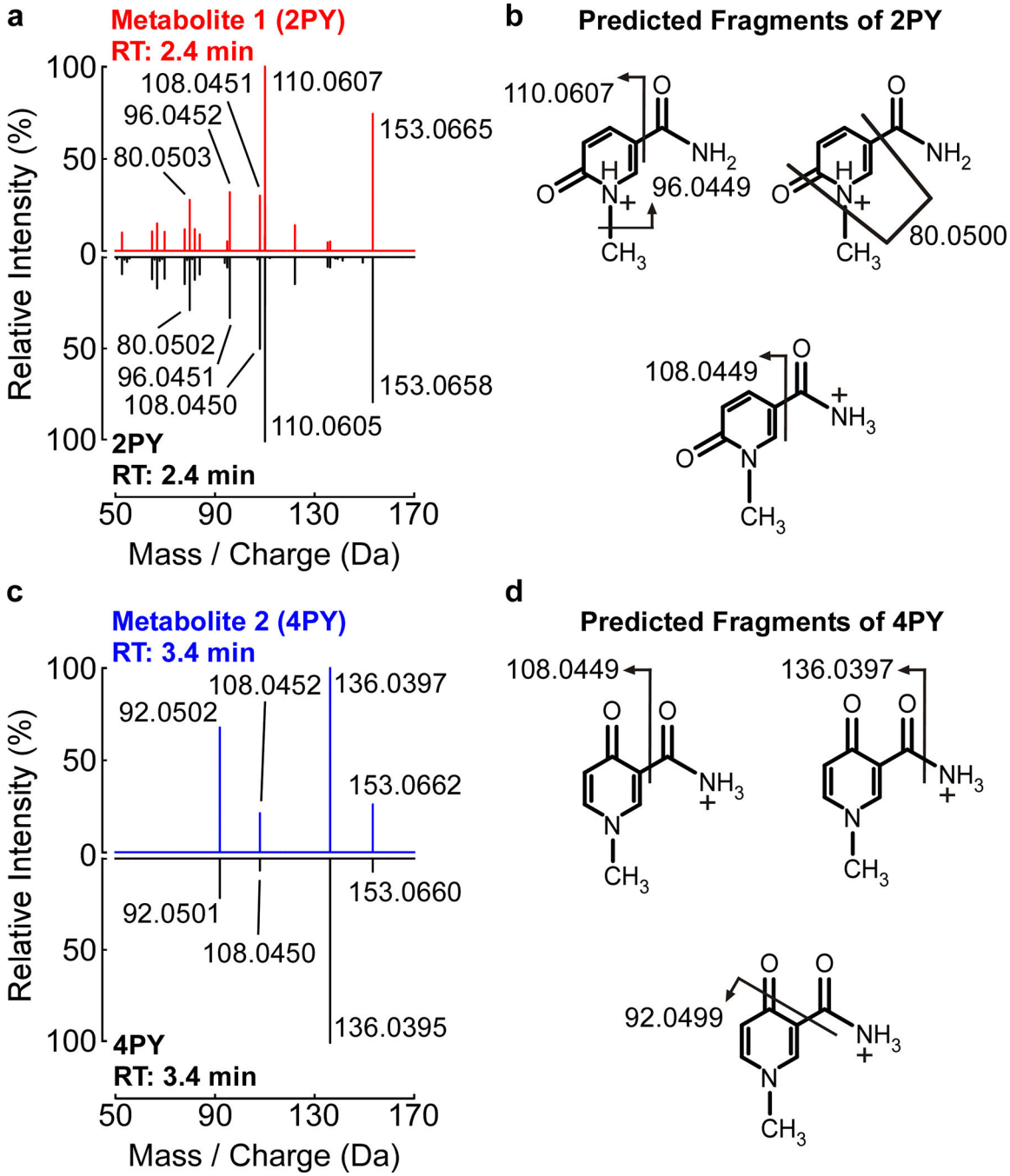

**Extended Data Fig. 5. Verifying the MACE-associated serum analyte with m/z = 153.0656 Da is comprised of 2PY and 4PY.**

The MACE-associated serum analyte with *m/z* = 153.0656 Da was resolved into two chromatographically separable structural isomers, 2PY and 4PY, using the new HPLC method. The two analytes have retention times of 2.4 min (metabolite 1; 2PY) and 3.4 min (metabolite 2; 4PY). (**a**) High resolution CID spectrum of serum metabolite 1 with retention time 2.4 min compared to synthetic 2PY (retention time 2.4 min). Peaks are labeled with their measured *m/z* in Da. (**b**) Sizes of predicted fragments of 2PY. Predicted fragments are labeled with their predicted *m/z* in Da. (**c**) CID spectrum of metabolite 2 with retention time 3.4 min compared to synthetic 4PY (retention time 3.4 min). Peaks are labeled with their measured *m/z* in Da. (**d**) Sizes of predicted fragments of 4PY. Predicted fragments are labeled with their predicted *m/z* in Da. Chemical synthesis of 2PY and 4PY is described in Supplemental Methods, and 1H-NMR spectra of synthetic material are shown in Supplemental Figures 1 and 2. Differences in *m/z* among predicted fragments and those observed for synthetic and serum 2PY and 4PY were within expected experimental error and are shown in Supplemental Table 6.

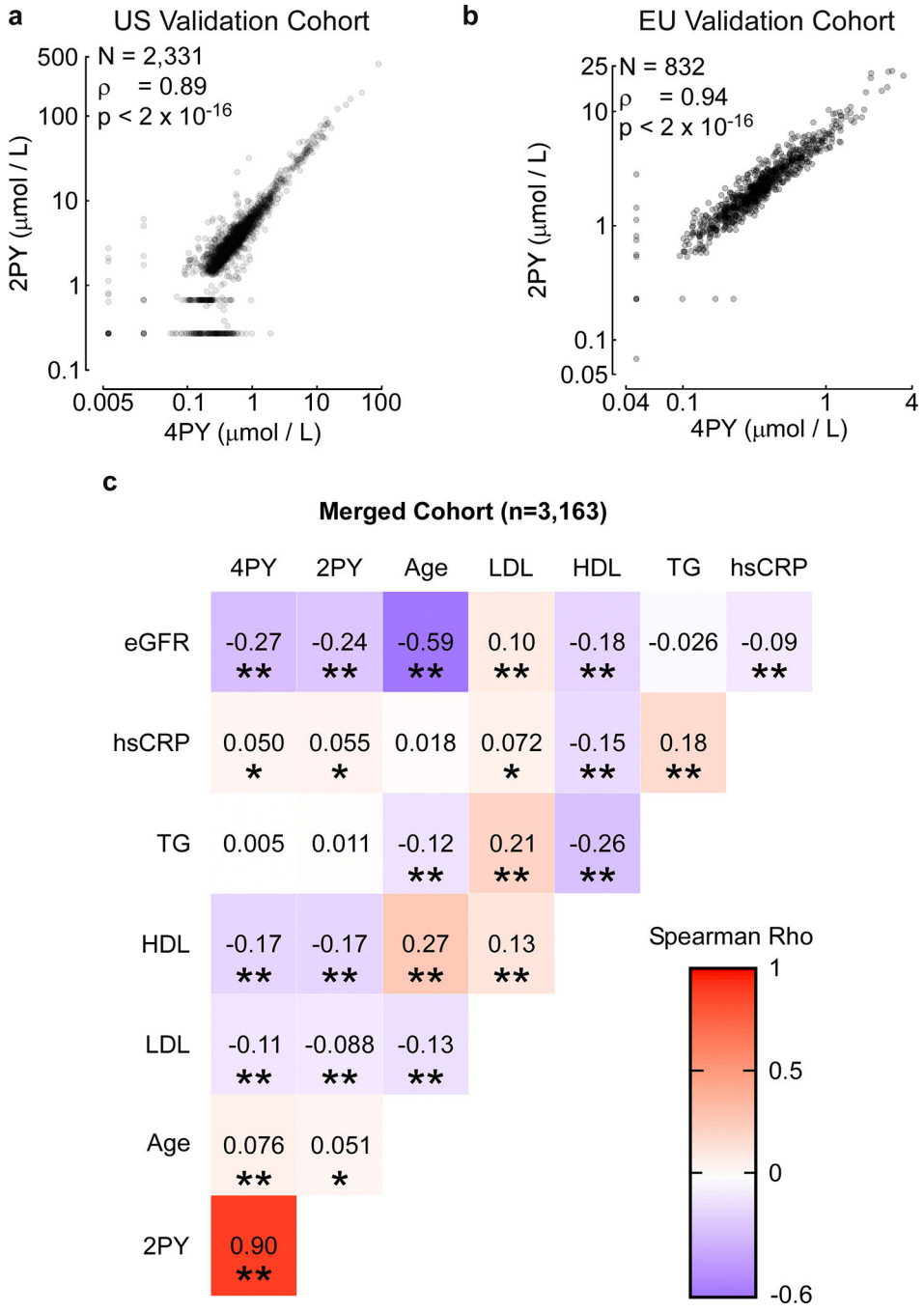


**Extended Data Fig. 6. Comparison of 2PY and 4PY levels in US and European Validation Cohorts**

(a - b) Serum levels of 2PY and 4PY were highly correlated in both the US and European Validation Cohorts. P values for Pearson correlations determined from t distributions with n-2 degrees of freedom ($P=1.2\times10^{-1757}$ for the US validation cohort and $P=2.1\times10^{-986}$ for the European validation cohort). P values for Spearman correlations determined with two-sided asymptotic t tests, and exact P values $<2\times10^{-16}$ could not be determined.(c) Spearman correlations among 2PY, 4PY, and risk factors for MACE. P values determined

with two-sided asymptotic t tests and adjusted for multiple testing using the false discovery rate method. Baseline clinical cohort characteristics are shown in Supplemental Table 2. ** p < 0.0001, * p < 0.05

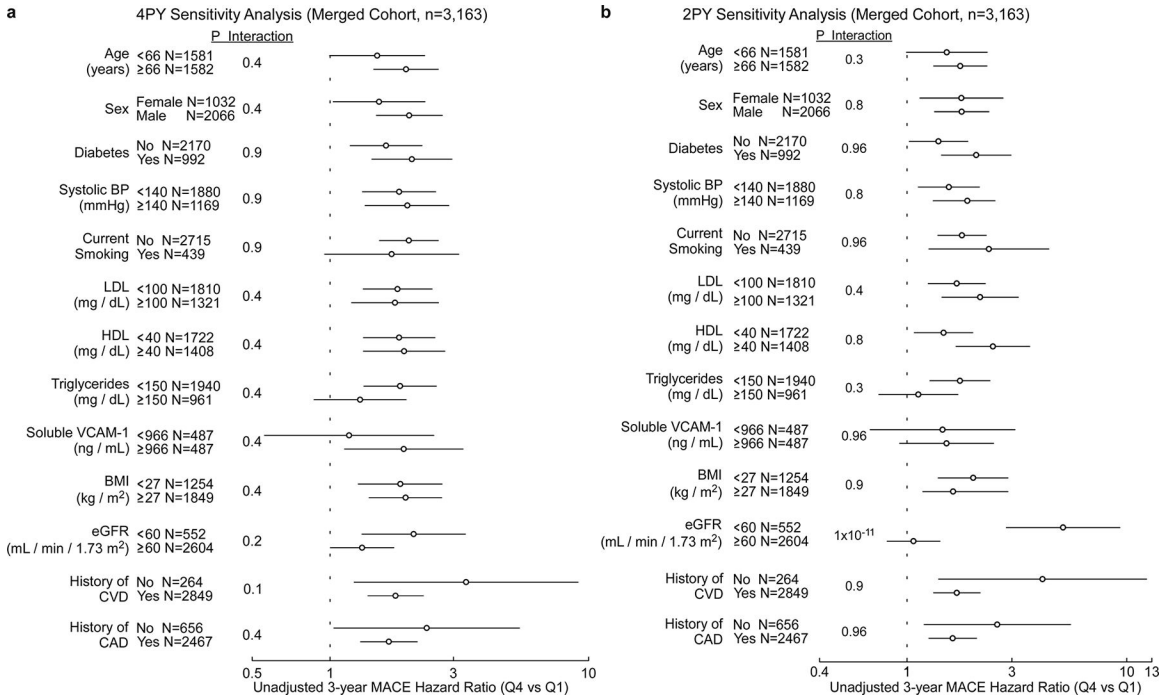


**Extended Data Fig. 7. Sensitivity analysis of 2PY and 4PY association with MACE in the merged cohort**

US and European Validation Cohorts were merged (n=3,163), and Hazard Ratio (quartile 4 (Q4) versus quartile 1 (Q1); open circle) for 4PY (panel a) and 2PY (panel b) association with MACE (3yr) risks for the indicated subgroups are shown. Baseline clinical cohort characteristics are shown in Supplemental Table 2. Symbols represent hazard ratios and error bars represent 95% confidence intervals. Ref, reference group. Interaction P values were determined with two-sided Wald tests and adjusted for multiple testing using the method of Benjamani and Hochberg. ** P < 0.0001; * P < 0.05

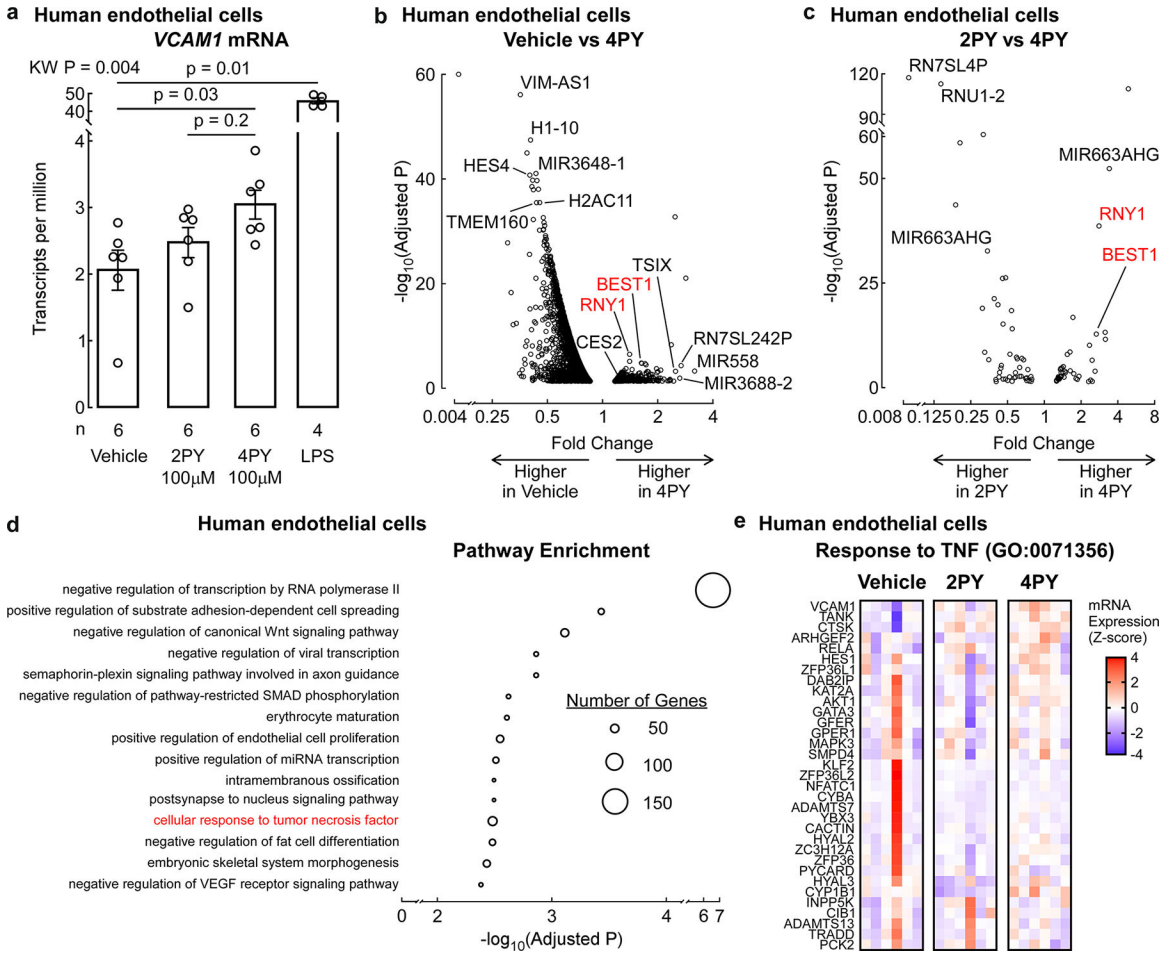


**Extended Data Fig. 8. Transcriptomic analysis of human endothelial cells exposed to 2PY or 4PY**

(**a**) Human endothelial cells were cultured with 2PY, 4PY, or vehicle control, and RNA was harvested after 4 hours. VCAM1 mRNA levels determined by RNA sequencing were elevated in 4PY-treated cells. The bar plot with error bars shows the mean plus or minus one standard error. P values were determined with two-sided Kruskal-Wallis (KW) and Wilcox tests. (**b**) Volcano plot shows differentially expressed genes for vehicle vs 4PY.(**c**) Differentially expressed genes for 2PY vs 4PY. Genes whose mRNA expression is impacted by 4PY compared to either control are shown in red. Fold change P values were determined using the log ratio test as implemented in edgeR and adjusted using the false discovery rate method. (**d**) Gene sets (Gene Ontology terms) whose member genes are enriched with the differentially expressed genes between vehicle and 4PY are shown. Dot size indicates the number of differentially expressed genes in the set. P values determined with two sided Fisher Exact tests and adjusted using the false discovery rate method. Only tip terms are shown, i.e. enriched GO terms with enriched child terms are not shown. All enriched GO terms are included in Source Data. (**e**) Genes associated with the cellular response to tumor necrosis factor (TNF) (shown in red in (**d**)) tend to have higher expression in 4PY-treated cells than vehicle- and 2PY-treated cells. Expression in transcripts per million transformed to Z-scores per gene.

## Extended Data Table 1:

Meta-analysis results for lead variants associated with circulating 2PY, 4PY and sVCAM-1 levels.

| Molecule | Lead SNP | Chr | Position | Nearest Gene | EA/ NEA | EAF | N | Z-score | Direction | P Value | P-het |
|---|---|---|---|---|---|---|---|---|---|---|---|
| **2PY** | rs10496731 | 2 | 135,597,628 | *ACMSD* | T/G | 0.56 | 37,453 | 14.7 | ++++++ | $1.6\times10^{-41}$ | $3\times10^{-5}$ |
| **4PY** | rs6430553 | 2 | 135,631,400 | *ACMSD* | C/T | 0.53 | 11,609 | 6.9 | +++ | $3.6\times10^{-12}$ | 0.2 |
| **sVCAM-1** | rs10496731 | 2 | 135,597,628 | *ACMSD* | T/G | 0.66 | 106,000 | 8.7 | ++++++ | $3.6\times10^{-18}$ | $9.9\times10^{-3}$ |

Individuals in the US validation cohort were genotyped. 2PY and 4PY were measured with stable isotope dilution LC/MS/MS and sVCAM-1 with ELISA. GWAS analyses for 2PY and 4PY were carried out in the US validation cohort and meta-analyzed with publicly available summary statistics from various multi-ancestry datasets. Meta-analysis was conducted with sample size weighting. Summary statistics for the lead variants for 2PY and 4PY levels within *ACMSD* (rs10496731 and rs6430553, respectively) are shown. The lead variant for 4PY levels, rs6430553, is in near perfect LD with rs10496731 ($r^2$=0.96), which was the second lowest P value for 4PY levels ($P=7.2\times10^{-12}$). Meta-analysis P values for all variants in the GWAS meta-analyses of 2PY and 4PY levels are shown in the Miami plot in Figure 4a. Citations and hyperlinks to all public datasets used for meta-analyses are shown in Supplemental Table 1. Genomic coordinates are based on GRCh37/hg19. Order of datasets for direction of effect of the effect allele (EA) are US Validation cohort, INTERVAL/EPIC, CLSA, METSIM, HCHS/SOL, and JHS for 2PY levels; US Validation cohort, TwinsUK/KORA, and Tohoku Medical MegaBank for 4PY levels; and UK Biobank, INTERVAL, FENLAND, DeCode, AGES, and the US Validation cohort for sVCAM-1 levels. In each previously published dataset, metabolite/protein levels were transformed prior to GWAS analyses as follows: INTERVAL/EPIC (residuals were calculated from natural log transformed values and standardized to have a mean of 0 and a standard deviation of 1); CLSA (natural log transformed values were standardized to have a mean of 0 and a standard deviation of 1); METSIM (residuals were calculated from inverse normal transformed values and inverse normal transformed again), HCHS/SOL (residuals were calculated and inverse normal transformed), JHS (residuals were calculated from natural log transformed values that were standardized to have a mean of 0 and a standard deviation of 1, followed by inverse normal transformation); TwinsUK/KORA (log base 10 transformation); and Tohoku Medical MegaBank (residuals were calculated from log transformed values and inverse normal transformed); UK Biobank (log base 2 transformed); FENLAND (log base 10 transformed); DeCode (residuals were calculated from inverse normal transformed values and inverse normal transformed again); AGES (Box-Cox transformation).

## Extended Data Table 2:

2PY, 4PY, and sVCAM-1 levels across associated genome wide significant variant (rs10496731) genotypes in the US Validation Cohort

| Analyte (P for trend) | Genotype (rs10496731) | Serum Concentration Median (IQR) |
|---|---|---|
| **4PY (P=0.02)** | | |
| | GG (n=582) | 0.458 (0.301–0.735) μmol/L |
| | GT (n=1089) | 0.463 (0.316–0.742) μmol/L |
| | TT (n=660) | 0.525 (0.330–0.774) μmol/L |
| **2PY (P=0.01)** | | |
| | GG (n=582) | 2.76 (1.73–4.46) μmol/L |
| | GT (n=1089) | 2.96 (1.86–4.76) μmol/L |
| | TT (n=660) | 3.21 (1.98–4.67) μmol/L |
| **sVCAM-1 (P=0.02)** | | |
| | GG (n=244) | 917 (729–1276) ng/mL |
| | GT (n=454) | 958 (747–1281) ng/mL |
| | TT (n=276) | 1030 (773–1372) ng/mL |

2PY and 4PY levels were measured in a sequential subset of the US Validation Cohort using stable isotope dilution LC/MS/MS. sVCAM-1 was measured by ELISA. The genetic variant rs10496731 was associated with 2PY, 4PY, and sVCAM-1 levels, and the direction of association was the same for all three analytes. Effect sizes of the genetic variant rs10496731 on 2PY, 4PY, and VCAM-1 levels were estimated with linear models of inverse normal transformed serum levels versus rs10496731 T allele copy number. Serum levels (median and interquartile range (IQR)) of each analyte across rs10496731 genotypes are shown. Increasing trends in 2PY, 4PY, and sVCAM-1 levels are shown with increasing number of rs10496731 T alleles. P values were determined with trend tests across the number of T alleles. The US Validation Cohort was included in the meta-analysis shown in Figure 4a and Extended Table 1. Baseline clinical characteristics are shown in Supplemental Table 2.

## Supplementary Material

Refer to Web version on PubMed Central for supplementary material.

## Acknowledgements

This work was supported by grants from the NIH (both NHLBI and the office of dietary supplements; R01HL103866 and P01HL147823, S.L.H.), (R01HL133169, R01HL148110, R01HL168493, and U54HL170326) (H.A.), Pilot Project Programs of the USC Center for Genetic Epidemiology and Southern California Environmental Health Sciences Center (P30ES007048) (J.A.H.) and the Deutsche Forschungsgemeinschaft (WI 5229/1–1) (M.W.). M.F. was supported in part by NIH training grants T32 HL134622 and T32 GM007250. A.H. is a participant in the BIH-Charité Advanced Clinician Scientist Program funded by the Charité – Universitätsmedizin Berlin and the Berlin Institute of Health. The LipidCardio Study (U.L. and I.D.) was partially supported by the Sanofi-Aventis Deutschland GmbH. We also gratefully acknowledge the UK Biobank Resource for providing access to their data under Application Number 33307.

## Data Availability

Source data for figures and tables included in the manuscript were deposited within Nature Medicine journal website as Source Data. The DNA sequences and sequence maps of AAVs used are available at https://doi.org/10.5281/zenodo.8357441. Summary statistics for the meta-analyses for 2PY and 4PY are also available at https://doi.org/10.5281/zenodo.8357441. There are restrictions to the availability of some of the clinical data generated in the present study for the US and EU Validation cohorts since the informed consent from research subjects in these studies does not permit sharing data outside each respective institution without authorization. Where permissible, the datasets generated and/or analyzed during the present studies are available from the corresponding author Stanley L. Hazen (hazens@ccf.org) on request. Individual level data used in the present study are available upon application to the UK Biobank (https://www.ukbiobank.ac.uk/).

## References

1. Virani SS et al. Heart Disease and Stroke Statistics - 2023 Update: A Report From the American Heart Association. Circulation vol. 147 (2023).
2. D'Agostino RB et al. General cardiovascular risk profile for use in primary care: The Framingham heart study. Circulation 117, 743–753 (2008). [PubMed: 18212285]
3. Ridker PM et al. Cardiovascular efficacy and safety of bococizumab in high-risk patients. N. Engl. J. Med. 376, 1527–1539 (2017). [PubMed: 28304242]
4. Sabatine MS et al. Evolocumab and clinical outcomes in patients with cardiovascular disease. N. Engl. J. Med. 376, 1713–1722 (2017). [PubMed: 28304224]
5. Pradhan AD, Aday AW, Rose LM & Ridker PM Residual inflammatory risk on treatment with PCSK9 inhibition and statin therapy. Circulation 138, 141–149 (2018). [PubMed: 29716940]
6. Bohula EA et al. Inflammatory and cholesterol risk in the FOURIER trial. Circulation 138, 131–140 (2018). [PubMed: 29530884]

7. Makarov MV, Trammell SAJ & Migaud ME The chemistry of the vitamin B3 metabolome. Biochemical Society Transactions (2019) doi:10.1042/BST20180420.
8. Wan P, Moat S & Anstey A Pellagra: A review with emphasis on photosensitivity. British Journal of Dermatology (2011) doi:10.1111/j.1365-2133.2010.10163.x.
9. Dietary Reference Intakes: The Essential Guide to Nutrient Requirements. (The National Academies Press, 2006). doi:10.17226/11537.
10. Stierman B et al. National Health and Nutrition Examination Survey 2017–March 2020 Prepandemic Data Files—Development of Files and Prevalence Estimates for Selected Health Outcomes. National Center for Health Statistics. 158, (2021)
11. Stamler J The Coronary Drug Project--findings with regard to estrogen, dextrothyroxine, clofibrate and niacin. Adv. Exp. Med. Biol. (1977) doi:10.1007/978-1-4613-4220-5_6.
12. Landmesser U The difficult search for a 'partner' of statins in lipid-targeted prevention of vascular events: The re-emergence and fall of niacin. Eur. Heart J. 34, 1254–1257 (2013). [PubMed: 23444398]
13. Lloyd-Jones DM Niacin and HDL cholesterol — time to face facts. N. Engl. J. Med. 371, 271–273 (2014). [PubMed: 25014692]
14. Landray MJ, Haynes R & Hopewell JC Effects of extended-release niacin with laropiprant in high-risk patients. N. Engl. J. Med. 371, 203–212 (2014). [PubMed: 25014686]
15. Boden WE, Field JLP-, Koprowicz, K. & Teo, K. Niacin in patients with low HDL cholesterol levels receiving intensive statin therapy. N. Engl. J. Med. 687–696 (2011) doi:10.1056/NEJMoa1107579.
16. Jenkins DJA et al. Supplemental vitamins and minerals for CVD prevention and treatment. J. Am. Coll. Cardiol. 71, 2570–2584 (2018). [PubMed: 29852980]
17. Li XS et al. Untargeted metabolomics identifies trimethyllysine, a TMAO-producing nutrient precursor, as a predictor of incident cardiovascular disease risk. JCI Insight (2018) doi:10.1172/jci.insight.99096.
18. Wang Z et al. Gut flora metabolism of phosphatidylcholine promotes cardiovascular disease. Nature 472, 57–65 (2011). [PubMed: 21475195]
19. Nemet I et al. A Cardiovascular disease-linked gut microbial metabolite acts via adrenergic receptors. Cell 180, 862–877.e22 (2020). [PubMed: 32142679]
20. Witkowski M et al. The artificial sweetener erythritol and cardiovascular event risk. Nat. Med. (2023). doi: 10.1038/s41591-023-02223-9
21. Abelson D, Boyle A, & Seligson H Identification of N'-methyl-4-pyridone-3-carboxamide in human plasma. J of Bio Chem. 238 (2), 717–718 (1962).
22. Menon R et al. Effect of the rate of niacin administration on the plasma and urine pharmacokinetics of niacin and its metabolites. J Clin Pharm. 47(6), 681–688 (2007).
23. Consortium GTEx. The Genotype-Tissue Expression (GTEx) project. Nat. Genet. 45 (6) 580–585, (2013) [PubMed: 23715323]
24. Sun B et al. Genomic atlas of the human plasma proteome. Nature. 558 (7708), 73–79 (2018). [PubMed: 29875488]
25. Gudjonsson G et al. A genome-wide association study of serum proteins reveals shared loci with common diseases. Nat Comm. 13 (1), 1–13 (2022).
26. Dansky HM et al. Adhesion of monocytes to arterial endothelium and initiation of atherosclerosis are critically dependent on vascular cell adhesion molecule-1 gene dosage. Arterioscler. Thromb. Vasc. Biol. 21, 1662–1667 (2001). [PubMed: 11597942]
27. Cybulsky MI et al. A major role for VCAM-1, but not ICAM-1, in early atherosclerosis. J. Clin. Invest. 107, 1255–1262 (2001). [PubMed: 11375415]
28. Sun B et al. Plasma proteomic associations with genetics and health in the UK Biobank. Nature. 622 (7982), 329–338 (2023). [PubMed: 37794186]
29. Aragam K et al. Discovery and systematic characterization of risk variants and genes for coronary artery disease in over a million participants. Nat. Genet. 54 (12), 1803–1815 (2022) [PubMed: 36474045]

30. Hartiala J et al. Genome-wide analysis identifies novel susceptibility loci for myocardial infarction. Eur. Heart J. 42 (9), 919–933 (2021) [PubMed: 33532862]
31. Mishra A et al. Stroke genetics informs drug discovery and risk prediction across ancestries. Nature. 611 (7934), 115–123 (2022) [PubMed: 36180795]
32. Chen F et al. Association among dietary supplement use, nutrient intake, and mortality among U.S. Adults. Ann. Intern. Med. 170, 604–613 (2019). [PubMed: 30959527]
33. Tyler J et al. Global Concerns with B Vitamin Statuses: Biofortification, Fortification, Hidden Hunger, Interactions, and Toxicity. Compr. Rev. Food Sci. Food Saf. 18(6), 1968–1964 (2019) [PubMed: 33336961]
34. Visseren FLJ et al. 2021 ESC Guidelines on cardiovascular disease prevention in clinical practice. Eur. Heart J. 42, 3227–3337 (2021). [PubMed: 34458905]
35. Mangione CM et al. Vitamin, mineral, and multivitamin supplementation to prevent cardiovascular disease and cancer: US Preventive Services Task Force recommendation statement. JAMA - J. Am. Med. Assoc. 327, 2326–2333 (2022).
36. Grundy SM et al. 2018 AHA/ACC/AACVPR/AAPA/ABC/ACPM/ADA/AGS/APhA/ASPC/NLA/PCNA Guideline on the Management of Blood Cholesterol: A Report of the American College of Cardiology/American Heart Association Task Force on Clinical Practice Guidelines. J. Am. Coll. Cardiol. 73, e285–e350 (2019). [PubMed: 30423393]
37. Teo KK et al. Extended-release niacin therapy and risk of ischemic stroke in patients with cardiovascular disease the atherothrombosis intervention in metabolic syndrome with low HDL/high triglycerides: Impact on global health outcome (AIM-HIGH) trial. Stroke (2013) doi:10.1161/STROKEAHA.113.001529.
38. United States Department of Agriculture Food Data Central. https://fdc.nal.usda.gov/ (2019).
39. United States Department of Agriculture Center for Nutrition Policy and Promotion. https://www.fns.usda.gov/USFoodSupply-1909-2010.
40. Elhassan YS et al. Nicotinamide riboside augments the aged human skeletal muscle NAD + metabolome and induces article nicotinamide riboside augments the aged human skeletal muscle NAD + metabolome and induces transcriptomic and anti-inflammatory signatures. Cell Reports 28, 1717–1728.e6 (2019). [PubMed: 31412242]
41. Trammell SAJ et al. Nicotinamide riboside is uniquely and orally bioavailable in mice and humans. Nat. Commun. 7, 1–14 (2016).
42. Yoshino M, Yohino J, Kayser B, Imai S-I & Klein S Nicotinamide mononucleotide increases muscle insulin sensitivity in prediabetic women. Science (80-. ). 373, 1224–1229 (2021).
43. Yi L et al. The efficacy and safety of β-nicotinamide mononucleotide (NMN) supplementation in healthy middle-aged adults: a randomized, multicenter, double-blind, placebo-controlled, parallel-group, dose-dependent clinical trial. GeroScience (2022) doi:10.1007/s11357-022-00705-1.
44. Chini E Effects of Vitamin B3 Derivative Nicotinamide Riboside (NR) in Bone, Skeletal Muscle and Metabolic Functions in Aging. NCT03818802.
45. Morten S-K Slow Age: Interventions to Slow Aging in Humans. NCT05593939.
46. Andriy Y & Mukli P The Effect of NAD Supplementation on Brain Vascular Health in Aging. NCT05483465
47. Martens CR et al. Chronic nicotinamide riboside supplementation is well-Tolerated and elevates NAD+ in healthy middle-Aged and older adults. Nat. Commun. 9, 1–11 (2018). [PubMed: 29317637]
48. Cantó C, Menzies KJ & Auwerx J NAD+ metabolism and the control of energy homeostasis: a balancing act between mitochondria and the nucleus. Cell Metabolism (2015) doi:10.1016/j.cmet.2015.05.023.
49. Lenglet A et al. N-methyl-2-pyridone-5-carboxamide (2PY) — Major metabolite of nicotinamide: An update on an old uremic toxin. Toxins (2016) doi:10.3390/toxins8110339.
50. Horwitt M, Harper A & Henderson L Niacin-tryptophan relationships for evaluating niacin equivalents. Am. J. Clin. Nutr. 34, 423–427 (1981). [PubMed: 6452053]
51. Pellicciari R et al. α-Amino-β-carboxymuconate-ε-semialdehyde decarboxylase (ACMSD) inhibitors as novel modulators of de novo nicotinamide adenine dinucleotide (NAD+) biosynthesis. J. Med. Chem. 61, 745–759 (2018). [PubMed: 29345930]

52. Katsyuba E et al. De novo NAD+ synthesis enhances mitochondrial function and improves health. Nature 563, 354–359 (2018). [PubMed: 30356218]
53. Yin X et al. Genome-wide association studies of metabolites in Finnish men identify disease-relevant loci. Nat Comm. 13 (1), 1664 (2022).
54. Hemani G et al. The MR-Base platform supports systematic causal inference across the human phenome. Elife. 7 (2018) DOI: 10.7554/eLife.34408
55. Ridker PM et al. Antiinflammatory therapy with canakinumab for atherosclerotic disease. N. Engl. J. Med. 377, 1119–1131 (2017). [PubMed: 28845751]
56. Ley K, Laudanna C, Cybulsky MI & Nourshargh S Getting to the site of inflammation: The leukocyte adhesion cascade updated. Nat. Rev. Immunol. 7, 678–689 (2007). [PubMed: 17717539]
57. Libby P Inflammation during the life cycle of the atherosclerotic plaque. Cardiovasc. Res. 117, 2525–2536 (2021). [PubMed: 34550337]
58. Marui N et al. Vascular cell adhesion molecule-1 (VCAM-1) gene transcription and expression are regulated through an antioxidant-sensitive mechanism in human vascular endothelial cells. J. Clin. Invest. 92, 1866–1874 (1993). [PubMed: 7691889]
59. Pigott R, Dillon LP, Hemingway IH & Gearing AJH Soluble forms of E-selectin, ICAM-1 and VCAM-1 are present in the supernatants of cytokine activated cultured endothelial cells. Biochem. Biophys. Res. Commun. 187, 584–589 (1992). [PubMed: 1382417]
60. Blankenberg S et al. Circulating cell adhesion molecules and death in patients with coronary artery disease. Circulation 104, 1336–1342 (2001). [PubMed: 11560847]

## Methods-only References

61. Koeth RA et al. Intestinal microbiota metabolism of L-carnitine, a nutrient in red meat, promotes atherosclerosis. Nat. Med. 19, 576–585 (2013). [PubMed: 23563705]
62. Brennan ML et al. Comprehensive peroxidase-based hematologic profiling for the prediction of 1-year myocardial infarction and death. Circulation 122, 70–79 (2010). [PubMed: 20566956]
63. König M et al. Cohort profile: Role of lipoproteins in cardiovascular disease - The LipidCardio study. BMJ Open 9, (2019).
64. Inker LA et al. New creatinine- and cystatin c–based equations to estimate GFR without race. N. Engl. J. Med. 385, 1737–1749 (2021). [PubMed: 34554658]
65. STROBE statement - Checklist of items that should be included in reports of observational studies (© STROBE Initiative). Int. J. Public Health 53, 3–4 (2008). [PubMed: 18522360]
66. Pluskal T, Castillo S, Villar-Briones A & Orešič M MZmine 2: Modular framework for processing, visualizing, and analyzing mass spectrometry-based molecular profile data. BMC Bioinformatics 11, (2010).
67. Li S et al. Predicting network activity from high throughput metabolomics. PloS Comput. Biol. 9, (2013).
68. Chong J et al. MetaboAnalyst 4.0: towards more transparent and integrative metabolomics analysis. Nucleic Acids Res. 46, W486–W494 (2018). [PubMed: 29762782]
69. Magnusson M et al. A diabetes-predictive amino acid score and future cardiovascular disease. Eur. Heart J. 34, 1982–1989 (2013). [PubMed: 23242195]
70. Du X et al. Relationships between circulating branched chain amino acid concentrations and risk of adverse cardiovascular events in patients with STEMI treated with PCI. Sci. Rep. 8, 6–13 (2018). [PubMed: 29311650]
71. Soda K, Kano Y & Chiba F Food polyamine and cardiovascular disease—an epidemiological study. Glob. J. Health Sci. 4, 170–178 (2012).
72. Lang R et al. Development of a hydrophilic liquid interaction chromatography-high- performance liquid chromatography-tandem mass spectrometry based stable isotope dilution analysis and pharmacokinetic studies on bioactive pyridines in human plasma and urine after coffee. Anal. Chem. 82, 1486 – 1497 (2010). [PubMed: 20073472]
73. Ruf S et al. Novel nicotinamide analog as inhibitor of nicotinamide N-methyltransferase. Bioorganic Med. Chem. Lett. 28, 922–925 (2018).

74. Chang CC et al. Second-generation PLINK: Rising to the challenge of larger and richer datasets. Gigascience 4, 1–16 (2015). [PubMed: 25838885]

75. Willer CJ, Li Y & Abecasis GR METAL: Fast and efficient meta-analysis of genomewide association scans. Bioinformatics 26, 2190–2191 (2010). [PubMed: 20616382]

76. Begum F, Ghosh D, Tseng GC & Feingold E Comprehensive literature review and statistical considerations for GWAS meta-analysis. Nucleic Acids Res. 40, 3777–3784 (2012). [PubMed: 22241776]

77. Pucci L et al. Tissue expression and biochemical characterization of human 2-amino 3-carboxymuconate 6-semialdehyde decarboxylase, a key enzyme in tryptophan catabolism. FEBS. 274 (3), 827–840 (2007).

78. Bycroft C et al. The UK Biobank resource with deep phenotyping and genomic data. Nature. 561 (7726), 203–209 (2018).

79. Burgess S Sample size and power calculations in Mendelian randomization with a single instrumental variable and a binary outcome. Int J Epidemiol. 43 (3), 922–929 (2014) [PubMed: 24608958]

80. Ram S et al. Pixelwise H-score: A novel digital image analysis-based metric to quantify membrane biomarker expression from immunohistochemistry images. PLoS One. 16 (9), e0245638 (2021) [PubMed: 34570796]

81. Xiao W et al. Immunometabolic endothelial phenotypes: Integrating inflammation and glucose metabolism. Circ Res. 129, 9–29 (2021). [PubMed: 33890812]

82. Bolger A et al. Trimmomatic: a flexible trimmer for Illumina sequence data. Bioinformatics. 30 (15), 2114–2120 (2014) [PubMed: 24695404]

83. Dobin A et al. STAR: ultrafast universal RNA-seq aligner. Bioinformatics. 29 (1), 15–21 (2013) [PubMed: 23104886]

84. Robinson M et al. edgeR: a Bioconductor package for differential expression analysis of digital gene expression data. Bioinformatics. 26 (1), 139–140 (2010) [PubMed: 19910308]

85. Alexa A, Rahnenfuhrer J, topGO: Enrichment Analysis for Gene Ontology. doi:10.18129/B9.bioc.topGO, R package version 2.54.0, https://bioconductor.org/packages/topGO

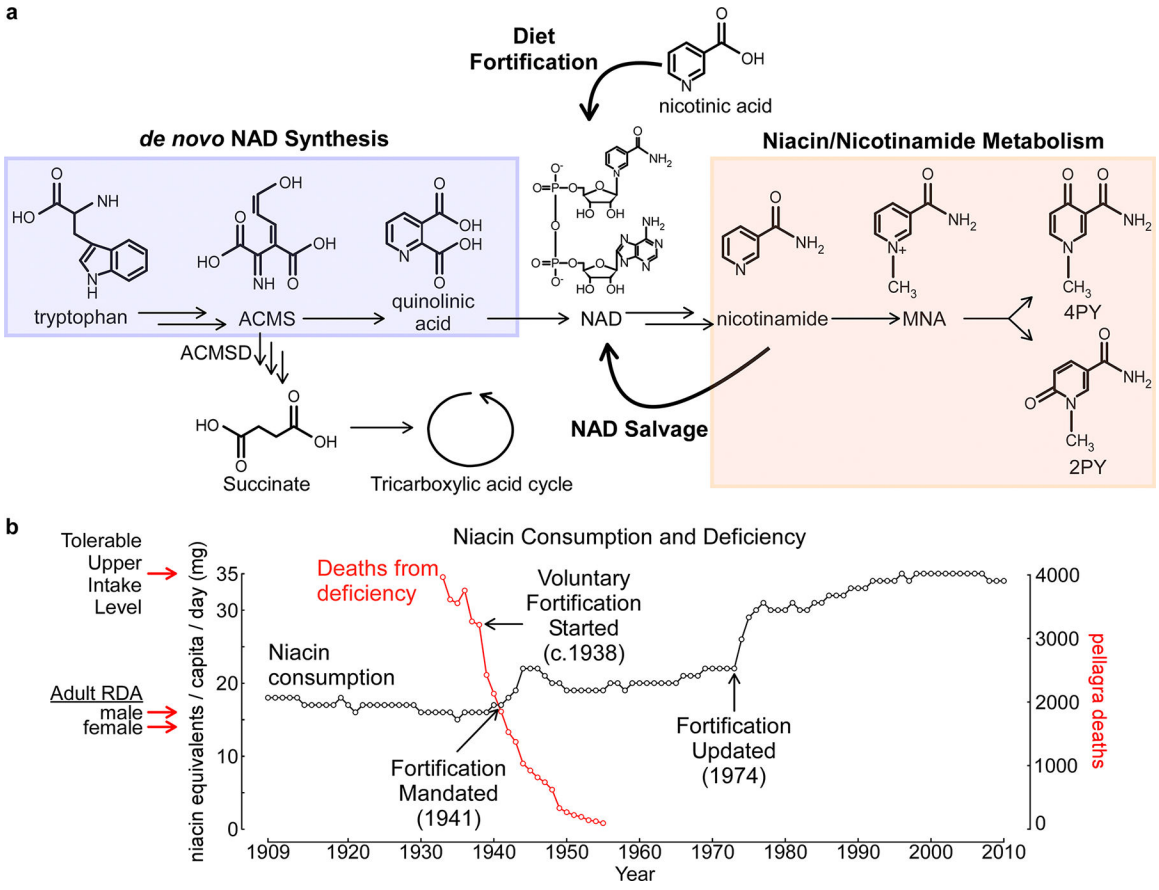


**Figure 1: Niacin is an essential micronutrient fortified in food staples beyond dietary requirements.**

(**a**) NAD, an essential cofactor, is synthesized via salvage or *de novo* pathways or from nicotinic acid, also known as niacin. Excess niacin or NAD is metabolized to 2PY and 4PY. The enzyme ACMSD regulates *de novo* NAD synthesis by diverting tryptophan to energy metabolism. (**b**) Historical estimated niacin equivalents per person per day for US adults are shown in black (USDA Center for Nutrition Policy and Promotion: Nutrient Content of the U.S. Food Supply 1909–2010). Historical pellagra deaths are shown in red (NCHS Vital Statistics 1933–1955). Recommended daily allowances (RDAs), the niacin consumption recommended by the National Academy of Sciences, is indicated for adult males and females, as well as the Tolerable Upper Intake Level, defined as the highest daily intake likely to pose no risk of skin flushing to almost all people (*Dietary Reference Intakes 2006*). ACMS, aminocarboxymuconate semialdehyde; NAD, nicotinamide adenine dinucleotide; MNA, N1-methyl-nicotinamide.

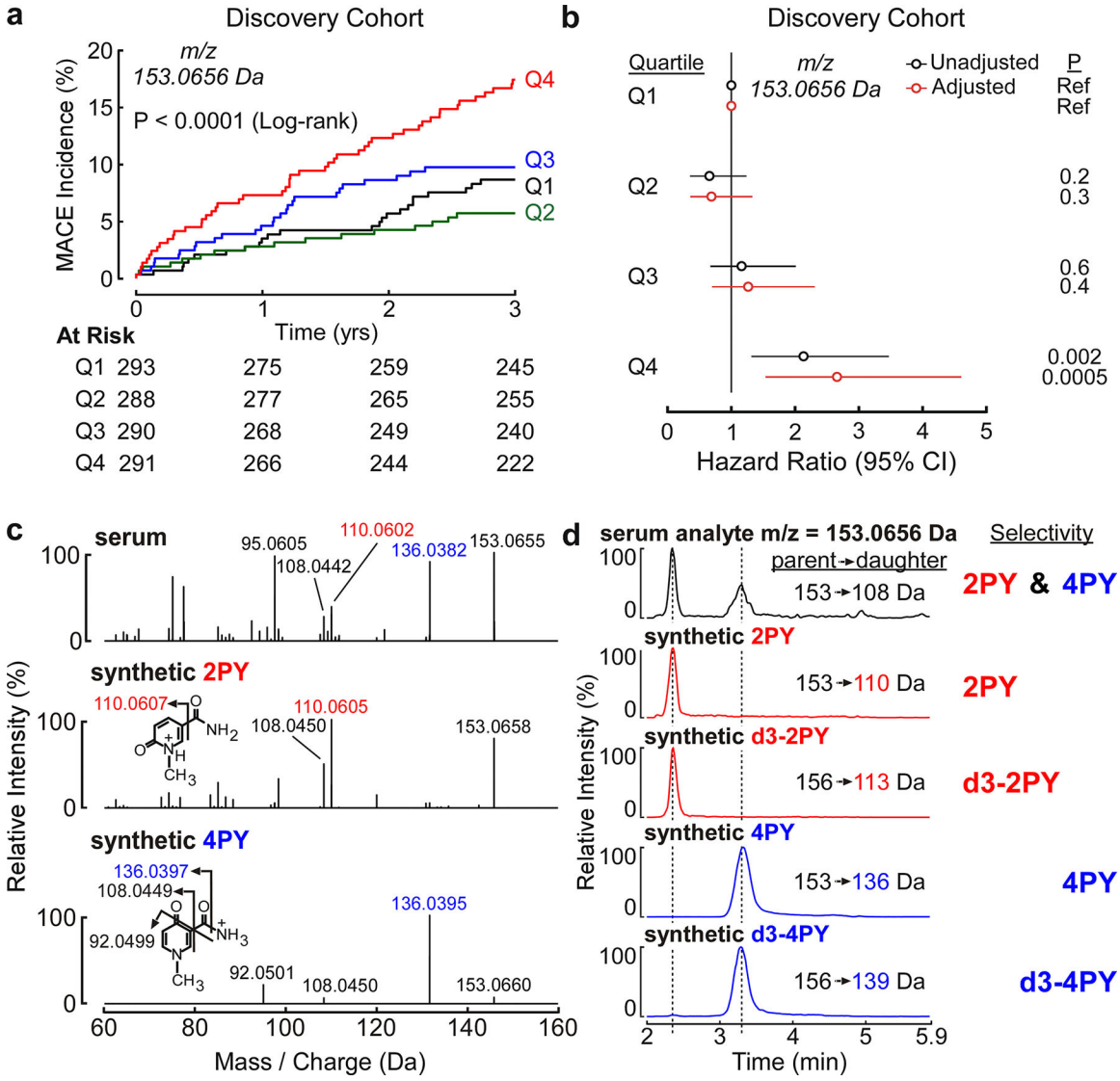


**Figure 2: Identification of the MACE-associated metabolite as2PY and 4PY, the terminal metabolites of niacin.**

(**a,b**) Kaplan-Meier estimates and two-sided log-rank test ($P=5.0\times10^{-5}$) (**a**) and hazard ratios (**b**) for MACE in the discovery cohort (n = 1,162) ranked by quartiles of a plasma analyte with *m/z* = 153.0656 Da. Cox models (unadjusted, open black circles) using the adjustments (adjusted, open red circles) traditional cardiovascular risk factors (age, sex, systolic blood pressure, LDL, HDL, triglycerides, diabetes status), hsCRP, current (active) smoking status, alcohol use, and education level. Symbols represent hazard ratios and error bars represent 95% confidence intervals. Ref, reference group. Hazard ratios for MACE-associated metabolites are shown in Supplemental Tables 3 and 4. (**c**) Collision-induced dissociation (CID) spectrum in positive-ion mode of the metabolite with *m/z* = 153.0656 Da in serum (upper) compared to CID spectra of synthetic 2PY (middle) and 4PY (lower). Molecular fragments characteristic of 2PY are shown in red; fragments characteristic of 4PY are shown in blue. (**d**) Demonstration of chromatography of parent-to-daughter ion transitions for plasma analytes with *m/z* = 153 Da and comparison to synthetic 2PY and

4PY and stable isotope-labeled d3–2PY and d3–4PY. Parent-to-daughter transitions selective for both 2PY and 4PY (153 → 108 Da) are shown in black; parent-to-daughter transitions selective for 2PY (153 → 110 Da) or d3–2PY (156 → 113 Da) are shown in red; parent-to-daughter transitions selective for 4PY (153 → 136 Da) or d3–4PY (156 → 139 Da) are shown in blueThree parent-to-daughter ion transitions were monitored for each analyte, and chromatograms for all transitions are shown in Extended Data Figure 4. Separate CID spectra were acquired for 2PY and 4PY using the HPLC method shown above (Extended Data Figure 5).

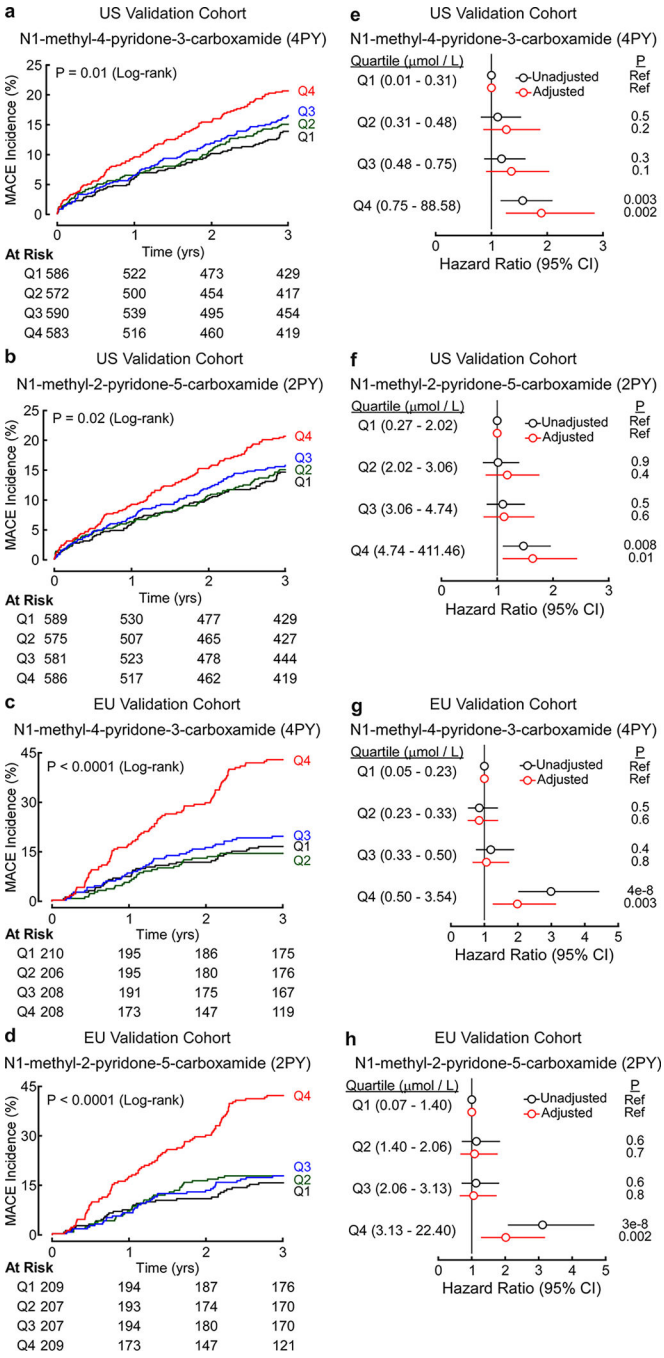


**Figure 3: Niacin metabolites 2PY and 4PY are associated with increased prospective MACE risk in two independent clinical cohorts.**

(**a**, **b**, **c**, **d**) Kaplan-Meier estimates are shown for the risk of incident 3-year MACE by quartiles of serum levels of 2PY and 4PY for the US validation (n=2,331) (**a**, **b**) and European validation (n=832) (**c**, **d**) cohorts. P values determined with two-sided log-rank tests (for the European validation cohort, $P=2.0\times10^{-12}$ and $P=1.9\times10^{-13}$ for the 2PY and 4PY, respectively). (**e**, **f**, **g**, **h**) Forest plots of Cox proportional hazard ratios for MACE by quartiles of serum levels of 2PY and 4PY are shown for the US (**e, f**) and the European

(**g**, **h**) validation cohorts. Cox models are shown (unadjusted, open black circles) using the adjustments (adjusted, open red circles) for traditional cardiovascular risk factors (age, sex, systolic blood pressure, LDL, HDL, triglycerides, diabetes status) hsCRP, current (active) smoking status, and alcohol use. The US validation cohort was additionally adjusted for education level. Symbols represent hazard ratios, and error bars represent 95% confidence intervals.

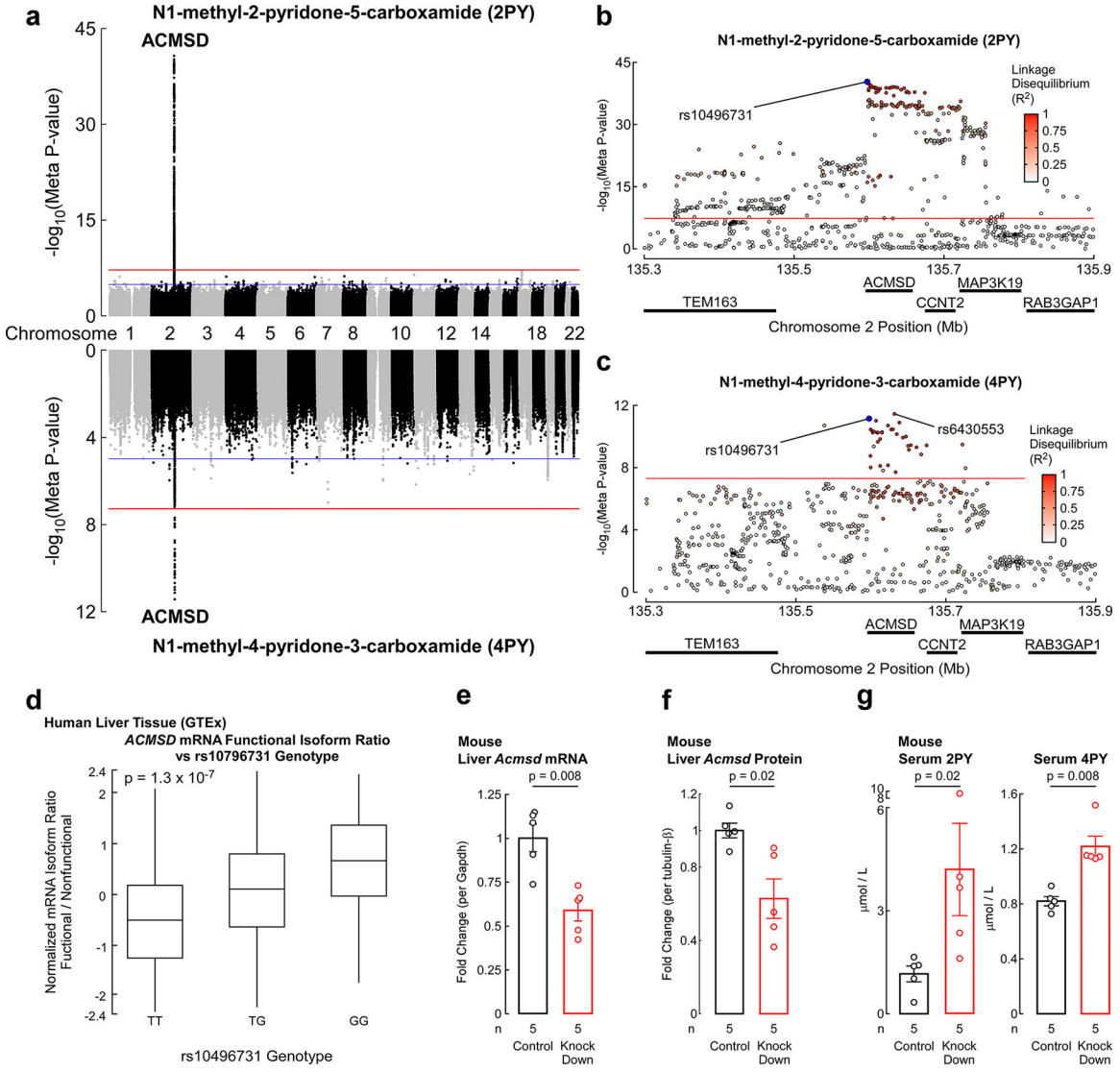


**Figure 4: The NAD synthesis gene *ACMSD* is associated with 4PY levels and vascular inflammation.**

(**a**) Miami plot of GWAS meta-analyses for levels of 2PY (top) and 4PY (bottom). Horizontal red and blue lines indicate thresholds for genome-wide significant ($P=5.0\times10^{-8}$) and suggestive ($P=5.0\times10^{-6}$) evidence for association, respectively. (**b** , **c**) Regional plots showing P values for variants within the chromosome 2 locus associated with 2PY (**b**) and 4PY (**c**) levels. Shades of red indicate the degree of linkage disequilibrium (LD) between the lead variants for 2PY (rs10496731, indicated in blue, $P=1.6\times10^{-41}$) and 4PY (rs6430553, $P=3.6\times10^{-12}$) and other variants at the locus. P values were determined with two-sided Z-score based meta-analysis with sample size weighting as implemented in METAL. P values are not adjusted for multiple testing. Horizontal red lines indicate the threshold for genome-wide significant ($P=5.0\times10^{-8}$) evidence for association. P values for association with 2PY and 4PY levels are shown for all variants for the US validation cohort in Supplemental Figure 3. (**d**) Relative expression data for the ratio of the two *ACMSD* transcript isoforms (functional:nonfunctional) stratified by rs10496731 genotype (n=208) were obatined from

the Genotype-Tissue Expression (GTEx) project. The singular P value obtained from GTEx were determined with two-sided Wald tests using linear regression analysis assuming an additive model with adjustment for sex, the top 5 genotyping principal components, sequencing platform, sequencing protocol, and 15 PEER (Probabilistic Estimation of Expression Residuals) factors. The singular obtained from GTEx P value was not adjusted for multiple testing. Central lines indicate medians, hinges indicate the interquartile range, and whiskers indicate the minima and maxima. (**e**) Liver *Acmsd* transcript fold-changes are shown for mice transduced with AAV expressing either scrambled shRNA (control) or shRNA targeting *Acmsd* mRNA transcripts (knockdown). (**f**) Quantification of ACMSD protein in mouse liver by Western blotting, shown fold-changes for control and knockdown mice. (**g**) Mouse serum 2PY (left) and 4PY (right) levels are shown for control and knockdown mice. Bar plots with error bars show the mean plus or minus one standard error. P values were determined with two-sided Wilcox tests.

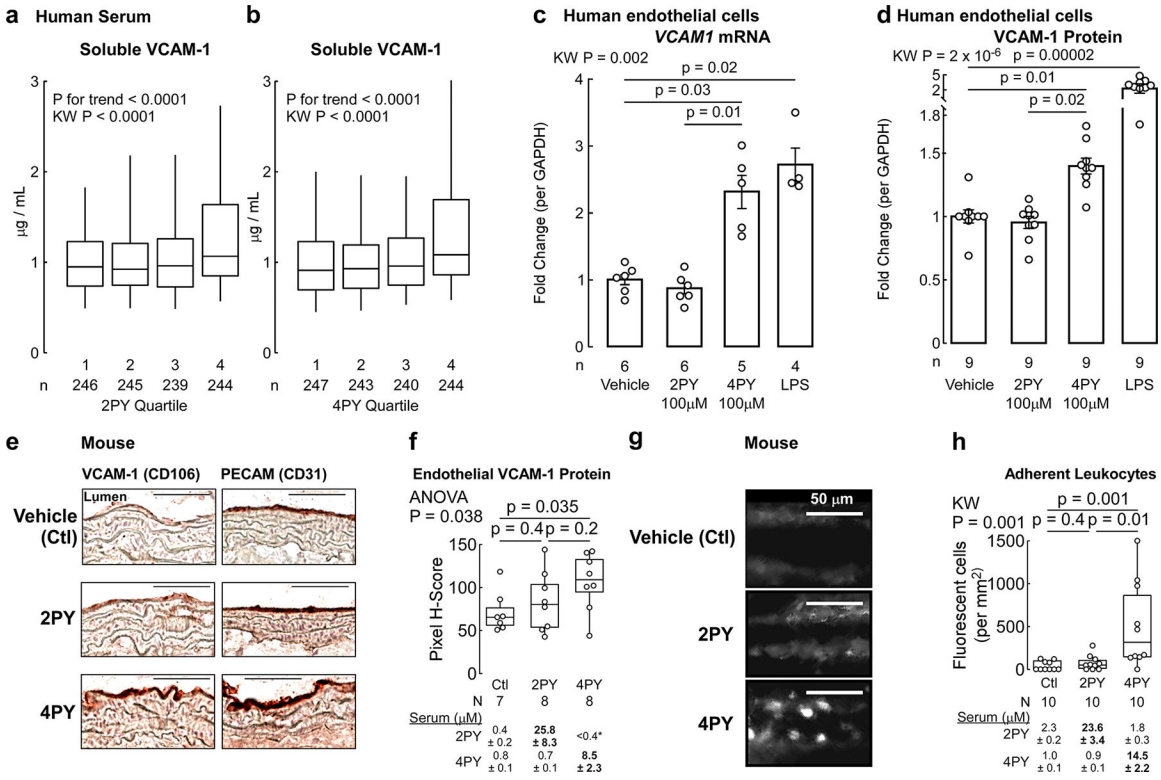


**Figure 5: The niacin metabolite 4PY enhances VCAM-1 expression and leukocyte adhesion *in vivo*.**

(**a,b**) Patient serum sVCAM-1 levels are shown stratified by quartiles of 2PY (**a**) and 4PY (**b**) serum levels within a subset of the US validation cohort (n=974). Central lines indicate medians, hinges indicate the interquartile range, and whiskers indicate 5$^{th}$ and 95$^{th}$ percentiles. P values were determined with two-sided trend tests ($P=8.0\times10^{-5}$ for 2PY and $P=4.0\times10^{-5}$ for 4PY) and Kruskal-Wallis tests ($P=2.5\times10^{-5}$ for 2PY and $P=4.8\times10^{-9}$ for 4PY). (**c,d**) For two separate experiments, *VCAM1* transcript fold changes, as determined by real-time quantitative PCR, (**c**) and VCAM-1 protein fold changes, as determined by Western blotting, (**d**) are shown following exposure to 2PY or 4PY, or vehicle control, or LPS as a positive control. Bar plots with error bars show the mean ± one standard error. P values were determined with the Kruskal-Wallis test with post-hoc Dunn's tests. Western blot images are shown in Supplemental Figure 4. (**e**) Immunohistochemical staining for VCAM-1 and a positive endothelial marker (PECAM) in aortas of mice after treatment with 2PY, 4PY, or vehicle control. Representative microscopy images are shown. Scale bar is 50 µm. (**f**) Endothelial VCAM-1 protein was quantified using pixel scoring, and the mean pixel H-score of three high-magnification fields is shown. P values determined with one-way ANOVA with post-hoc student t tests. (**g**) Intravital microscopy of auricular venules of mice treated with 2PY or 4PY or vehicle control. Representative microscopy images are shown. Scale bar is 50 µm. (**h**) Numbers of adherent leukocytes determined with intravital microscopy. The mean of three venules per animal is shown. Endpoint serum concentrations of 2PY and 4PY are shown as mean ± standard error, and bold text indicates concentrations in 2PY- and 4PY-treated mice that are statistically different from those of control animals. For boxplots, the central line represents the median, the upper and lower hinges represent the

interquartile range, and whiskers represent the smallest or largest value within 1.5 times the interquartile range of the lower or upper hinge. P values determined using Kruskal-Wallis Test with post-hoc Dunn's tests. *, samples below the lower limit of detection (LOD) were assigned a value of ½ the LOD.

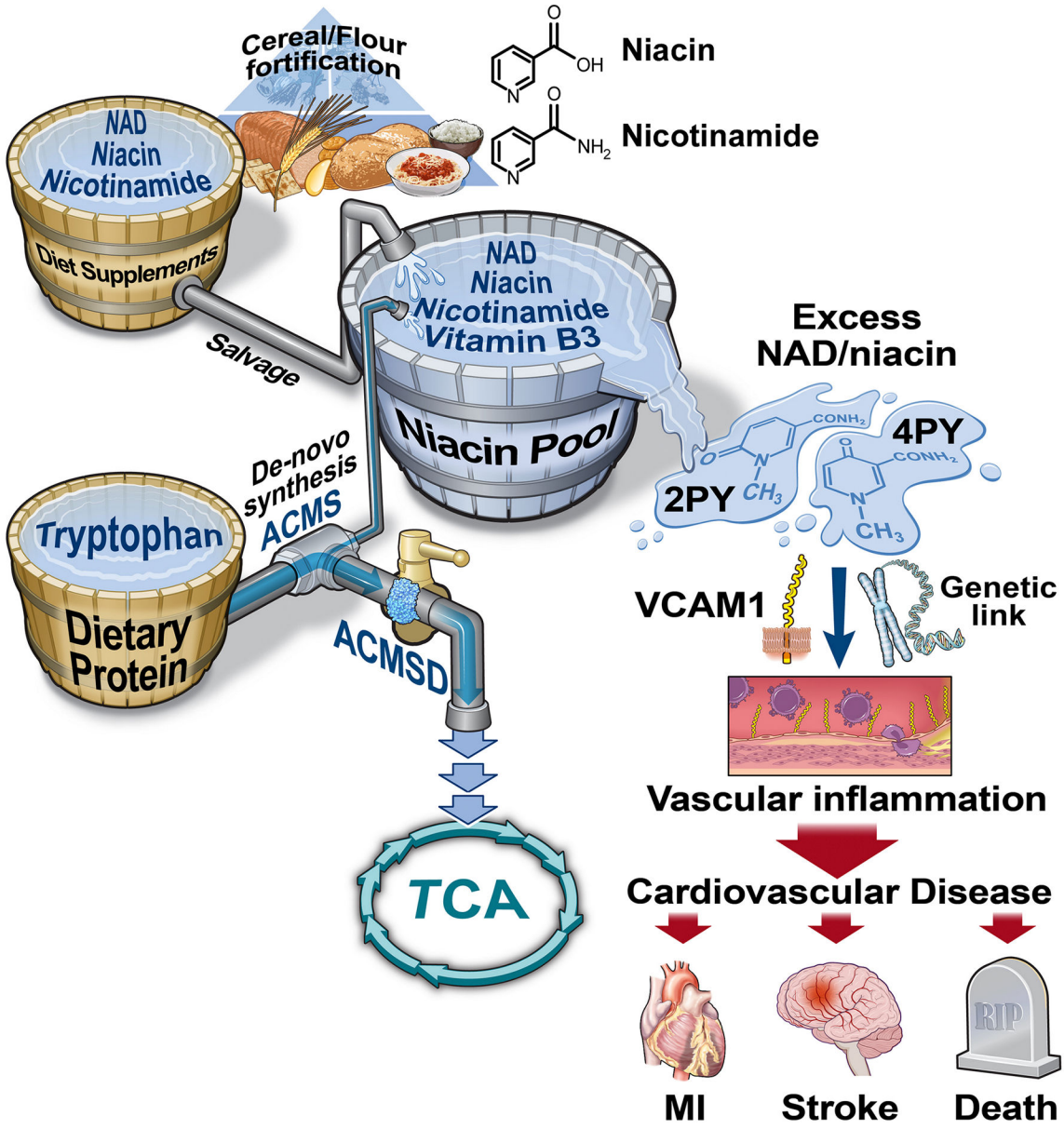


**Figure 6: Niacin metabolites 2PY and 4PY are associated with increased VCAM-1 expression and residual cardiovascular event risk.**

Dietary niacin, which is fortified in food staples, contributes to the NAD pool via the salvage pathway, which is the major contributor to the NAD pool. In the de-novo pathway, tryptophan-NAD conversion is regulated by the enzyme ACMSD, which diverts tryptophan to the tricarboxylic acid (TCA) cycle. The gene encoding ACMSD contains genetic variants associated with 2PY, 4PY, and sVCAM-1 levels. Excess NAD is metabolized to 2PY and 4PY, and 4PY induces mRNA and protein expression of VCAM-1 as well as leukocyte adherence to the vascular wall. VCAM-1 is also genetically linked to and correlated with 2PY and 4PY levels in circulation. Elevated circulating levels of 2PY, 4PY, and VCAM-1 are all associated with increased residual risk of prospective MACE (myocardial infarction [MI], stroke, and death).